Modeling and Stability Analysis of SMIB system incorporating a VSC based HVDC link

A thesis presented to

The Academic Faculty

By

Chowdhury Andalib Bin Karim (092463)

Muhammad Rizvi Hossain (092471)

Md. Ibrahim Adham (092466)

In partial fulfillment

Of the requirements for the degree

Bachelor of Science (B.Sc.)

In

Electrical and Electronic Engineering

Islamic University of Technology

October, 2013

Modeling and Stability Analysis of SMIB system incorporating a VSC based HVDC link

A Thesis Presented to
The Academic Faculty

By

Chowdhury Andalib Bin Karim (092463)
Muhammad Rizvi Hossain (092471)
Md. Ibrahim Adham (092466)

Approved by
Ashik Ahmed

…….
Ashik Ahmed
Thesis Supervisor
Assistant Professor
Dept. of Electrical & Electronic Engineering, IUT

……..
Prof. Dr. Md. Shahid Ullah
Head of the Department
Dept. of Electrical & Electronic Engineering, IUT

Member:

…… ……
Chowdhury Andalib Bin Karim Muhammad Rizvi Hossain

……..
Md. Ibrahim Adham

Islamic University of Technology (IUT)
The Organization of the Islamic Cooperation (OIC)
Gazipur-1704, Dhaka, Bangladesh
October-2013

ABSTRACT

In recent years, power demand has increased substantially while the expansion of power generation and transmission facilities have been severely limited due to limited resources and environmental restrictions. As a consequence, power systems are being operated under high stress level conditions. These operating conditions have negative impact on system stability, reliability, controllability and security margins. The instability problem causes fluctuation in different parameters of power system which may cause great damage or even cause complete shutdown of the system.

FACTS devices and HVDC transmissions have emerged as solution to help power system to increase the stability margins. HVDC transmissions are of particular interest since its ability to independently control active and reactive power.

This paper discusses the impact of HVDC on power system stability. Different disturbances are applied in order to analyze dynamic response of the system. HVDC tends to make the system unstable if the setting of a line is not changed during and after a disturbance. A control mechanism has been proposed to strengthen the system stability.

The establishment of the linearized Phillips-Heffron model of a system equipped with VSC-HVDC link is presented in this paper. On the basis of linearized Phillips-Heffron model, open loop eigenvalues are calculated and state space equations are used to design damping controller. Finally an optimal lead lag controller is designed to enhance damping of low frequency oscillations. The effectiveness and performance of the proposed controller is demonstrated through eigenvalue analysis and non linear time domain simulations. Moreover, the performance of the controller with different control input signals is evaluated and most effective control input is determined.

Simulation results carried by MATLAB show the effectiveness of proposed strategy for enhancing dynamic stability.

ACKNOWLEDGEMENTS

The undergraduate thesis, ***"Modeling and Stability Analysis of SMIB system incorporating a VSC based HVDC link"*** has been written for the completion of Bachelor of Science degree at Islamic University of Technology, Bangladesh. This thesis work and writing has been done during the year 2013 under the supervision of ***Ashik Ahmed, Assistant Professor of EEE Department***.

We would like to pay our special thanks and express our deepest gratitude to ***Prof. Dr. Md. Shahid Ullah,*** head of the department & ***Ashik Ahmed***, thesis supervisor for their constant guidance, help and encouragement to our work. Without their support it would have been impossible to complete such a task successfully.

We are also grateful to all of our will-wishers, who provided their perpetual support towards accomplishing this task successfully. Finally, we beg pardon and apologize for the faults and any unintentional mistakes that might be recurred in this thesis paper even after all the care that was taken.

Contents

Chapter 1: Power system Stability

1.1. Introduction

The stability of the power system is defined as “the ability of an electric power system, for a given initial operating condition, to regain a state of operating equilibrium after being subjected to a physical disturbance, with most system variables bounded so that practically the entire system remains intact” [1]. According to above definition it is clear that if system fails to get operating equilibrium then it will be called instable. There are many kind of instabilities exists in the modern power systems (such as voltage, frequency etc.) and accordingly the different stabilization methods are used. The stabilization processes basically works by compensation of the causing the instability in past this is done by connecting and disconnecting the capacitor, inductors or combination of both after that synchronous condenser, saturated reactor, thyristor controlled reactor, fixed capacitor thyristor controlled reactor, thyristor switched capacitor were used; but in present days this is performed by more advanced devices like STATCOM, VSC, TCSC etc. these devices evolves the intelligent controlling and fast switching power devices like MOSFET and IGBT the capability of fast switching makes them feasible for providing precise and smooth controlling. The intelligent controlling is performed by the complex calculations which are done by either analog circuits or microprocessors. Although analog devices performed well but in recent past developments in the semiconductor technology makes the digital controllers as first choice because of their capabilities and lower cost.

1.2. Types of instabilities in power system

The classification to be introduced here is based on the physical mechanism being the main driving force in the development of the associated instability.

Power System Stability (PSS) problems may be classified as [1]:

• Angle Stability

• Voltage Stability

• Frequency (Mid- and Long-Term) Stability

Each category can be divided to [1]:

- Small-Signal (Dynamic) Stability: Determines if system remains in synchronism following a small disturbance (e.g., small load and/or generation variations).

- Transient Stability: Determines if system remains in synchronism following a major disturbance (e.g., transmission fault, sudden load change, loss of generation, line switching). The transient stability can further be divided into two classes.
- First-Swing Stability: for 1st second after a system fault (simple generator model & no control model).
- Multi Swing Stability: system analysis over long period of time (more sophisticated machine model).

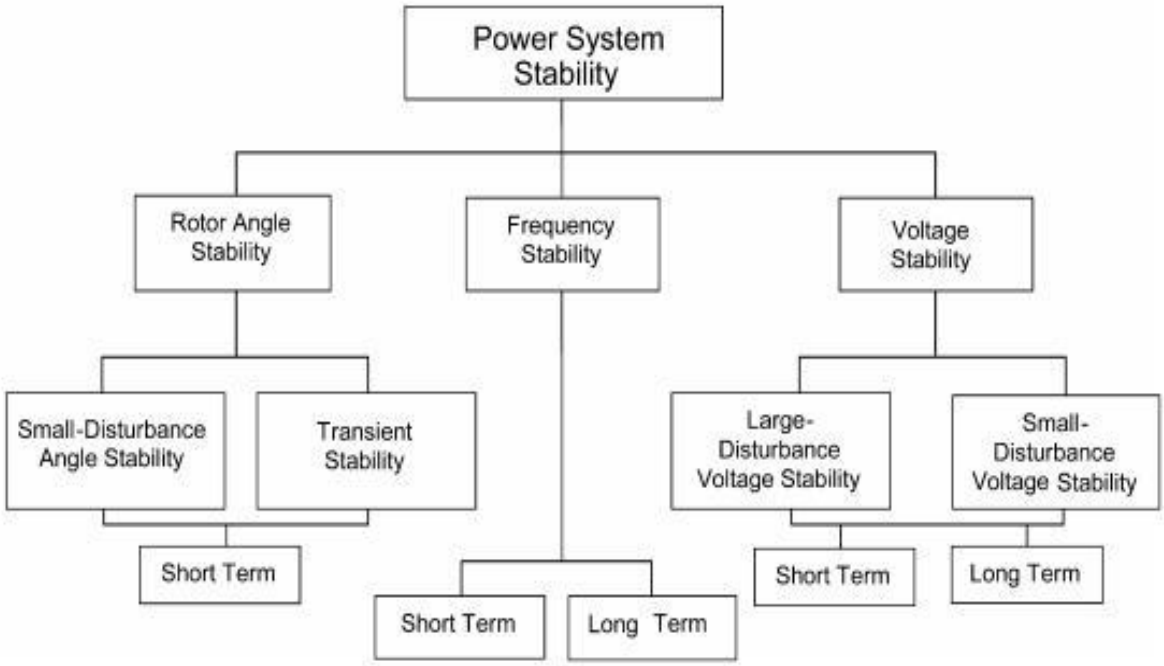

Figure 1.1: Classification of power system stability

1.2.1. Rotor angular or synchronous stability

The rotor angle stability problem involves the study of the electromechanical oscillations inherent in power systems. A fundamental factor in this problem is the manner in which the power outputs of synchronous machines vary as their rotor angles change. The mechanism by which interconnected synchronous machines maintain synchronism with one another is through restoring forces, which act whenever there are forces tending to accelerate or decelerate one or more machines with respect to other machines. Under steady-state conditions, there is equilibrium between the input mechanical torque and the output electrical torque of each machine, and the speed remains constant. If the system is perturbed, this equilibrium is upset,

resulting in acceleration or deceleration of the rotors of the machines according to the laws of motion of a rotating body. If one generator temporarily runs faster than another, the angular position of its rotor relative to that of the slower machine will advance. The resulting angular difference transfers part of the load from the slow machine to the fast machine, depending on the power angle relationship. This tends to reduce the speed difference and hence the angular separation. The power angle relationship, as discussed above, is highly nonlinear. Beyond a certain limit, an increase in angular separation is accompanied by a decrease in power transfer; this increases the angular separation further and leads to instability. For any given situation, the stability of the system depends on whether or not the deviations in angular positions of the rotors result in sufficient restoring torques. It should be noted that loss of synchronism can occur between one machine and the rest of the system, or between groups of machines, possibly with synchronism maintained within each group after separating from each other.

1.2.2. Voltage stability

When it comes to reactive power balance the situation is not as clear and simple as concerning active power. There is always a balance between “produced” and “consumed” reactive power in every node of a network. This is in fact a direct consequence of Kirchoff’s first current law. When one talks about imbalance in this context we mean that the injected reactive power is such, normally too small, that the voltage in the node cannot be kept to acceptable values. (At low load the injected reactive power could be high resulting in a too high voltage, possibly higher than the equipment might be designed for. This is of course not desirable but it could usually be controlled in such a way that no instabilities develop.) When we talk about imbalance in this case we thus mean that the injected reactive power differs from the desired injected reactive power, needed to keep the desired voltage. If this imbalance gets too high, the voltages exceed the acceptable range.

1.2.3. Frequency stability

Frequency stability refers to the ability of a power system to maintain steady frequency following a severe system upset resulting in a significant imbalance between generation and load. It depends on the ability to maintain/restore equilibrium between system generation and load, with minimum unintentional loss of load. Instability that may result occurs in the form of sustained frequency swings leading to tripping of generating units and/or loads. Severe system upsets generally result in large excursions of frequency, power flows, voltage, and other system variables, thereby invoking the actions of processes, controls, and protections that are not modeled in conventional transient stability or voltage stability studies. These processes may be very slow, such as boiler dynamics, or only triggered for extreme system conditions, such as volts/Hertz protection tripping generators. In large interconnected power systems, this type of situation is most commonly associated with conditions following splitting of systems into islands. Stability in this case is a question of whether or not each island will reach a state of operating equilibrium with minimal unintentional loss of load. It is determined by the overall response of the island as evidenced by its mean frequency, rather than relative motion of machines. Generally,

frequency stability problems are associated with inadequacies in equipment responses, poor coordination of control and protection equipment, or insufficient generation reserve.

1.3. Power system stability improvement strategies

The stability of power systems depends on the active and reactive power balance between generation and load within the system. Losing this balance leads to loss of system integrity leading to system collapse which has damaging impact on daily economic activities. In order to avoid such devastating impacts there should be effective mechanism for maintaining this balance [2]. These days different solution mechanisms are continued to be employed by power utilities worldwide for insuring this balance and bring about improved system stability. Strategies for power system stability improvement are implemented at two levels as shown in the chart in figure 1.2. The first is at generating units through the action of power system stabilizers (PSSs), automatic voltage regulators (AVRs) and other supplementary controllers. The power utilities worldwide are currently implementing PSSs and AVRs as excitation controllers to enhance power system stability. However, due to limited capacity and large system voltage variations introduced during disturbances upon utilizing them, they are getting insufficient to create system wide influences [2]. The other solution group is through the application of FACTS devices and HVDC controls at the transmission level.

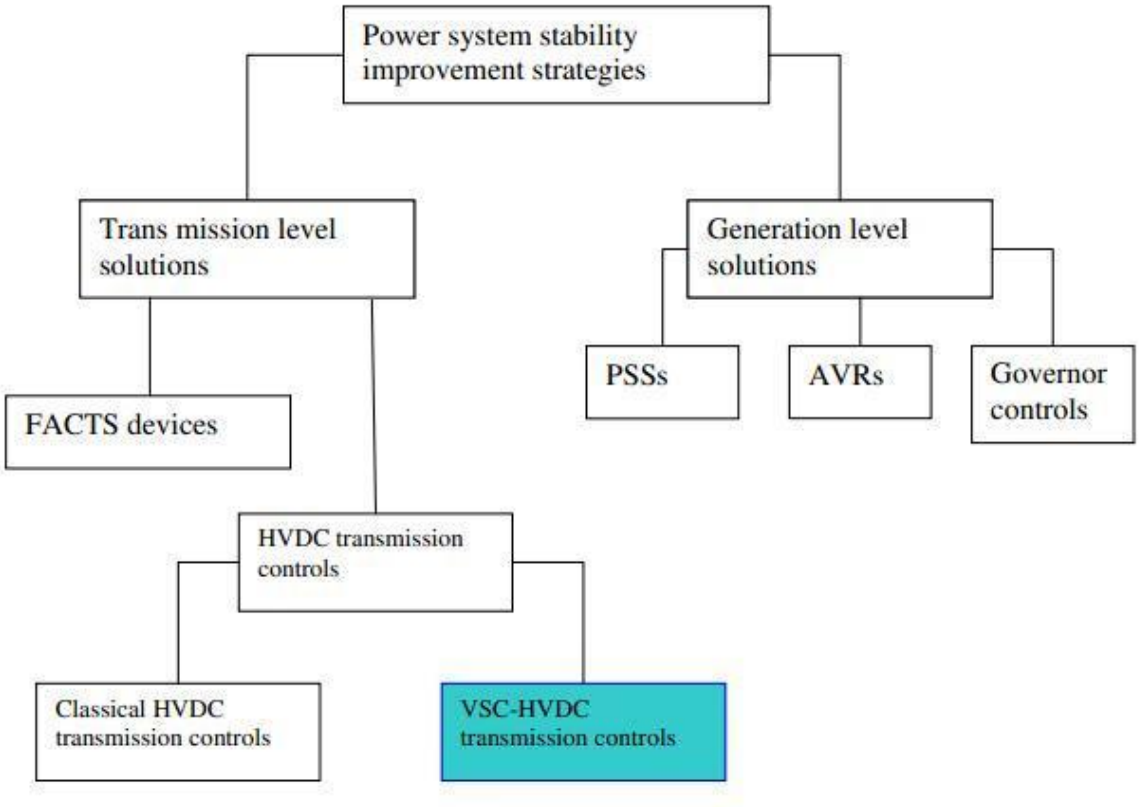

Figure 1.2: power system stability improvement strategies

1.3.1 Flexible Alternating Current Transmission Systems (FACTS)

FACTS is defined by the IEEE as a power electronic based system and other static equipment that provide control of one or more AC transmission system parameters to enhance controllability and increase power transfer capability.

There are two groups of FACTS devices. The first group employs conventional thyristor-switched capacitors and reactors, and quadrature tap-changing transformers. This includes the Static Var Compensator (SVC), the Thyristor- Controlled Series Capacitor (TCSC), and the Thyristor-Controlled Phase Shifter (TCPS). The second group utilizes gate turn-off (GTO) thyristor-switched converters as voltage source converters (VSCs). This group contains Static Synchronous Compensator (STATCOM), the Static Synchronous Series Compensator (SSSC), the Unified Power Flow Controller (UPFC), and the Interline Power Flow Controller (IPFC) [2].

FACTS devices have been mainly used for solving various power system steady state control problems such as voltage regulation, power flow control, and transfer capability enhancement. As supplementary functions, damping the interarea modes and enhancing power system stability using FACTS controllers have been extensively studied and investigated. These regulatory tasks are accomplished trough appropriate reactive power compensation, or by series capacitive compensation of line inductances, or by phase angle shifting.

However it is not found to be cost-effective to install FACTS devices for the sole purpose of power system stability enhancement.

1.3.2 HVDC as stability improvement tool

HVDC based on line commutated converters have limitations that restricted the range of its application. VSC-HVDC on the other hand provides the power system with many important benefits which greatly improve system stability. The following are advantages of VSC-HVDC over classical HVDC [2].

• Independent Active and reactive power control and power quality control.

• High quality voltage waveform generation, thereby reducing filtering requirements.

• Unlike LCC-HVDC unlimited power reversal.

• Reduced power losses in interconnected AC systems.

• Increased transfer capacity in the existing system.

• Powerful damping control using P and Q simultaneously.

• Fastest restoration after blackouts.

In VSC-HVDC transmission system reactive power is controlled at each terminal independent of one another. This reactive power control can be used for dynamic voltage regulation to support the interconnected AC systems following contingencies. This helps to increase the over all system power transfer levels and improve system dynamic performance.

VSC-HVDC can be an attractive option to efficiently and timely relieve network constraints, thus reducing the need for building new HVAC lines. In addition, VSC-HVDC may offer a lower environmental impact and a smaller territorial footprint due to a compact station design. Also, both HVDC and VSC-HVDC offer undergrounding possibilities by using cables as a transmission medium.

Chapter 2:
Overview of HVDC Transmission Systems

2.1. Introduction

High Voltage Direct Current (HVDC) technology has characteristics that make it es-pecially attractive for certain transmission applications. HVDC transmission has been widely recognized as being advantageous for long-distance bulk-power delivery, asynchronous interconnections, and long submarine cable crossings. Therefore, HVDC has been in use for more than 50 years and has remained a niche technology.

HVDC has proved to be a reliable and valuable transmission media for electrical energy in favor of its technical superiority compared with HVAC transmission. None the-less, a comprehensive HVDC/HVAC system planning approach is not commonly found within utilities and therefore full HVDC technology's advantage is not being taken. HVDC projects often provide strategically important enhancements and cost effective additions to AC networks. However, HVDC transmission is perceived to be expensive, difficult to integrate in an AC network, to require highly skilled personnel to operate and maintain, and to have high power losses [3].

Recent developments in energy policies and stronger environmental lobbies have a significant impact on the design and construction of electrical power transmission networks, and could provide a number of opportunities for HVDC transmission. The number of HVDC projects committed or under consideration globally has increased in recent years reflecting a renewed interest in this mature technology. This new converter design has broadened the potential range of HVDC transmission to include applications for underground, offshore, economic replacement of reliability-must-run generation, and voltage stabilization. This broader range of applications has contributed to the recent growth of HVDC transmission [3].

2.2. Environmental Aspects of HVDC

An HVDC transmission system is basically environment-friendly because improved energy transmission possibilities contribute to a more efficient utilization of existing power plants.

1. Visual impact and space requirements:

An HVDC cable uses significantly less land than an HVAC OHL. An HVDC transmission with an OHL requires less space per MW than traditional AC solutions. The tower's visual impact is therefore reduced. If a cable is used, the only visual impact is the converter stations. However, the size of these stations in comparison with traditional AC stations may have larger visual impact to be dealt with [3].

2. Electric and magnetic fields:

The magnetic field produced by a DC line is stationary while in the AC case it is alternating, which can cause inducing body currents. This result in fewer restrictions for the magnetic field in the HVDC line. The electric field is less severe in DC lines compared to AC ones since there is no steady state displacement current in the DC case. VSC-HVDC cables' magnetic fields are almost eliminated with the bipolar system. However, an undersea HVDC line can cause disturbances to magnetic compass systems on vessels crossing the cable.

3. Radio interference:

The harmonics created in switching processes by converters cause disturbances in the kHz and MHz regions. An appropriate shielding of valves minimizes this problem. This makes the radio interference comparable with AC solutions. Radio interference is normally a minor problem in transmission systems.

4. Audible noise:

An underground DC cable naturally has no audible noise emission. Audible noise from transmission line corona is most noticeable when OHL conductors are wet in foggy weather conditions. Consequently, buildings construction close to OHLs might be restricted. Audible noise mostly depends on line's voltage and its design specifications.

2.3 Technical Merits of HVDC

The DC link technical advantages over an AC one are [3]:

- A DC link allows power transmission between AC networks with different frequencies, or systems which can not be synchronized for other reasons;
- Inductive and capacitive parameters do not limit either the transmission capacity or the maximum length of a DC OHL or DC cable. Additionally, the conductor cross section is fully utilized because there is no skin effect;
- There is no phase shift between current and voltage. With AC, this flaw has to be eliminated using controlling elements in an energy-intensive process;
- HVDC solutions may have lower power losses especially for large distances. The power loss in a HVDC converter station is higher than that in an AC substation because of the conversion between AC and DC and the harmonics produced by this process. However, the total power loss in a HVDC transmission line can be 50% to 70% of that in an equivalent HVAC one. Moreover, when VSC-HVDC underground transmission is used inside an AC-grid, the transmission system can be more optimally operated that leads to lower electrical losses;
- Fast modulation of DC transmission power can be used for power oscillations damping in an AC grid and thus improving system's stability;

2.4. Economical Merits of HVDC

As world energy resources are normally decentralized from the ever increasing energy consumption, long HVDC transmissions are a particularly interesting area for the future. A key characteristic of HVDC transmissions is higher power transfers in fewer lines than an equivalent AC solution. Furthermore, a major constraint when designing traditional AC transmission lines over long distances is the significant inductance such a line will have. The effects of both the line inductance and capacitance have to be compensated along the AC line and this adds costs for long distances. The frequency is zero for DC; hence the inductance is irrelevant. Subsequently, an overhead DC line with its towers can be designed to be less costly per km than an equivalent AC solution, if both the investment and capitalization of total energy losses are considered.

Whenever long-distance transmission is discussed, the concept of "break-even distance" frequently arises. This is where the savings in line costs offset the higher converter station costs. Bipolar HVDC lines use only two insulated sets of conductors rather than three. This results in narrower rights-of-way, smaller transmission towers, and lower line losses than with AC lines of comparable capacity. A rough approximation of savings in line construction is about 30%. Furthermore, long-distance AC lines usually require intermediate switching stations and reactive power compensation which increases the overall AC transmission cost.

HVDC converter stations at both ends are more costly than equivalent AC terminals, thus, an economical break-even distance arises, as illustrated in Figure 2.1.The break-even distance, where the HVDC solution becomes more economical than an equivalent AC, greatly depends on land conditions and project specifications. The reasons for choosing HVDC are generally economic and not technical. Power system stability improvements and environmental circumstances may, however, also be reasons for using this technology. Favorable economics of bulk power transmission with HVDC together with its controllability make it an interesting alternative or complement to AC transmission. Therefore, thanks to HVDC transmission's economical, technical, and environmental merits, the strategies for future transmission infrastructure development go clearly towards HVDC applications.

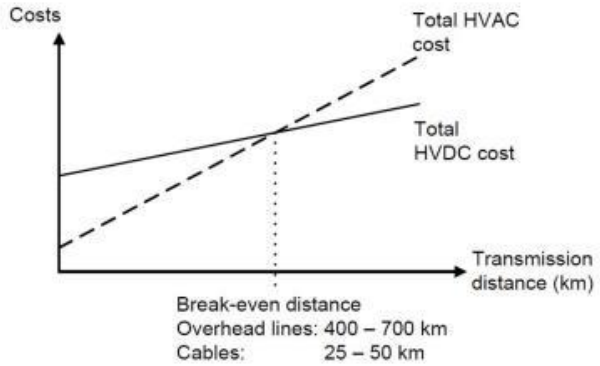

Figure 2.1: Cost against transmission distance for HVDC and HVAC system

2.5 HVDC Application

HVDC transmission applications can be broken down into different basic categories. Although the rationale for selection of HVDC is often economic, there may be other reasons for its selection. HVDC may be the only feasible way to interconnect two asynchronous networks, reduce fault currents, utilize long UGC circuits, bypass network congestion, share utility rights of-way without degradation of reliability, and to mitigate environmental concerns. Therefore, the following HVDC applications are presented:

Long-distance bulk power transmission

HVDC transmission systems often provide a more economical alternative to AC transmission for long distance bulk power delivery from remote resources such as hydroelectric developments, mine-mouth power plants, or large-scale wind farms. Higher power transfers are possible over longer distances using fewer lines with HVDC than with AC transmission. Typical HVDC lines utilize a bipolar configuration with two independent poles, one at a positive voltage and the other at a negative voltage with respect to ground. Bipolar HVDC lines are comparable to a double circuit AC line since they can operate at half power with one pole out of service but require only one-third the number of insulated sets of conductors as for double circuit AC line.

Underground and submarine cable transmission

The charging current in HVAC cables makes transmissions over long distances impractical. In order to keep voltage levels and power losses within reasonable limits, HVAC transmission requires reactive power compensation equipment along the cable. Such equipment adds cost to the link, and in some cases can not be implemented. If how-ever the cable is fed with HVDC, the large capacitance is irrelevant since the charging current is frequency dependent.

Nonetheless, there is no physical restriction limiting the distance or power level for HVDC underground or submarine cables. For these types of HVDC transmission cables, considerable savings in both installation and losses costs are yielded. For a given cable conductor, HVDC cable's losses can be about half those of AC ones. AC cables clearly require more conductors (three phases), carry the reactive current component, present skineffect, and carry induced currents in the cable sheath and armor. With this cable system, the need to balance unequal loadings or the risk of post contingency overloads often requires the use of series-connected reactors or phase shifting transformers. These potential problems do not exist with a controlled HVDC cable system.

Extruded HVDC cables with prefabricated joints used with VSC-based transmission are lighter, more flexible, and easier to splice than the mass-impregnated oil-paper cables MINDs used for conventional HVDC, thus making them more conducive for land cable applications where transport limitations and extra splicing costs can drive up installation costs. Thus, long distance underground with DC VSC-based transmission is comparatively economically feasible for use in areas with rights-of-way constraints, or subjected to licence difficulties or delays compared with OHLs.

Asynchronous ties

With HVDC transmission systems, interconnections can be performed between asynchronous networks for more economic or reliable system operation. Asynchronous systems' interconnections allow mutual benefit while providing a buffer between both AC systems. These interconnections often use back to back converters with no transmission line. Asynchronous HVDC links act as an effective "firewall" against propagation of cascading outages in any network from passing to another one.

Offshore transmission

Self-commutation, dynamic voltage control, and black-start capability allow compact VSC-HVDC transmission to serve isolated loads on islands or offshore production platforms over long-distance submarine cables. This capability can eliminate the need for running expensive local generation or provide an outlet for offshore generation such as that from wind. VSCs can operate at variable frequency to efficiently drive large compressor or pumping loads using high-voltage motors. Therefore, VSC-based HVDC transmission allows efficient use of either long-distance land or submarine cables. It also provides reactive support to the wind generation complex unit.

Multi-terminal systems

Most HVDC systems are of point to point HVDC transmission type with a converter station at each end. The use of intermediate taps is rare. Conventional HVDC transmission uses voltage polarity reversal to change the power flow direction. Polarity reversal requires no special switching arrangement for two terminal system where both terminals reverse polarity by a control action with no switching. However, special DC side switching arrangements are required for polarity reversal in multi-terminal systems where they may be desired to reverse the power direction at a tap while maintaining the same power direction on remaining terminals. For a bipolar system, this can be done by connecting the converter to the opposite pole. Notably, VSC-HVDC reverses power through the reversal of current direction rather than voltage polarity.

Power delivery to large urban areas

Power supply to large cities depends on local generation and power import capability. Local generation is often older and less effcient than newer units located remotely. However, older less effcient units located near the city center must often be dispatched out of merit because they must be run for voltage support or reliability due to inadequate transmission. Air quality regulations may limit the availability of these units. New transmission into large cities is diffcult to site due to right-of-way limitations and land use constraints. Compact VSC-based underground transmission circuits can be placed on existing dual-use rights-of-way to bring in power as well as to provide voltage support allowing a more economical power supply without compromising reliability. The receiving terminal acts as a virtual generator delivering power, supplying voltage regulation and reserving dynamic reactive power. Stations are compact and housed mainly indoors, making siting in urban areas somewhat easier. Furthermore, dynamic voltage support offered by VSCs can often increase the adjacent AC transmission capability.

Stabilization in power systems

HVDC links can be used within synchronous AC systems to improve the power flow control from one part of the system to another, and consequently, to prevent large cascading failures or even blackouts in the grid. System stability can be improved since the HVDC link provides damping torque.

2.6. Different HVDC Schemes

A. Back-To-Back Converters

The "Back-to-back" indicates that the rectifier and inverter are located in the same station. Back-to-back converters are mainly used for power transmission between adjacent AC grids which cannot be synchronized. They can also be used within a meshed grid in order to achieve a defined power flow.

B. Monopolar Long-Distance Transmissions

For very long distances and in particular for very long sea cable transmissions, a return path with ground/sea electrodes will be the most feasible solution. In many cases, existing infrastructure or environmental constraints prevent the use of electrodes. In such cases, a metallic return path is used in spite of increased cost and losses.

C. Bipolar Long-Distance Transmissions

A bipolar is a combination of two independent poles in such a way that a common low voltage return path, if available, will only carry a small unbalance current during normal operation. This configuration is used if the required transmission capacity exceeds that of a single pole. It is also used if requirement to higher energy availability or lower load rejection power makes it necessary to split the capacity on two poles. During maintenance or outages of one pole, it is still possible to transmit part of the power. More than 50% of the transmission capacity can be utilized, limited by the actual overload capacity of the remaining pole, while require only one-third the insulated sets of conductors compared to a double-circuit AC line. Other advantages of a bipolar solution over a solution with two monopoles are reduced cost, due to one common or no return path, and lower losses.

1) Bipolar With Ground Return Path:

This is a commonly used configuration for a bipolar transmission system. The solution provides a high degree of flexibility with respect to operation with reduced capacity during contingencies or maintenance, upon a single-pole fault, the current of the sound pole w ill be taken over by the ground return path and the faulty pole will be isolated. Following a pole outage caused by the converter, the current can be commutated from the ground return path into a metallic return path provided by the HVDC conductor of the faulty pole.

2) Bipolar With Dedicated Metallic Return Path For Monopolar Operation:

If there are restrictions even to temporary use of electrodes, or if the transmission distance is relatively short, a dedicated LVDC metallic return conductor can be considered as an alternative to a ground return path with electrodes.

3) Bipolar Without Dedicated Return Path For Monopolar Operation:

A scheme without electrodes or a dedicated metallic return path for monopolar operation will give the lowest initial cost; Monopolar operation is possible by means of bypass switches during a converter pole outage, but not during an HVDC conductor outage. A short bipolar outage will follow a converter pole outage before the bypass operation can be established. Fig. 2.2 shows different HVDC Schemes [4].

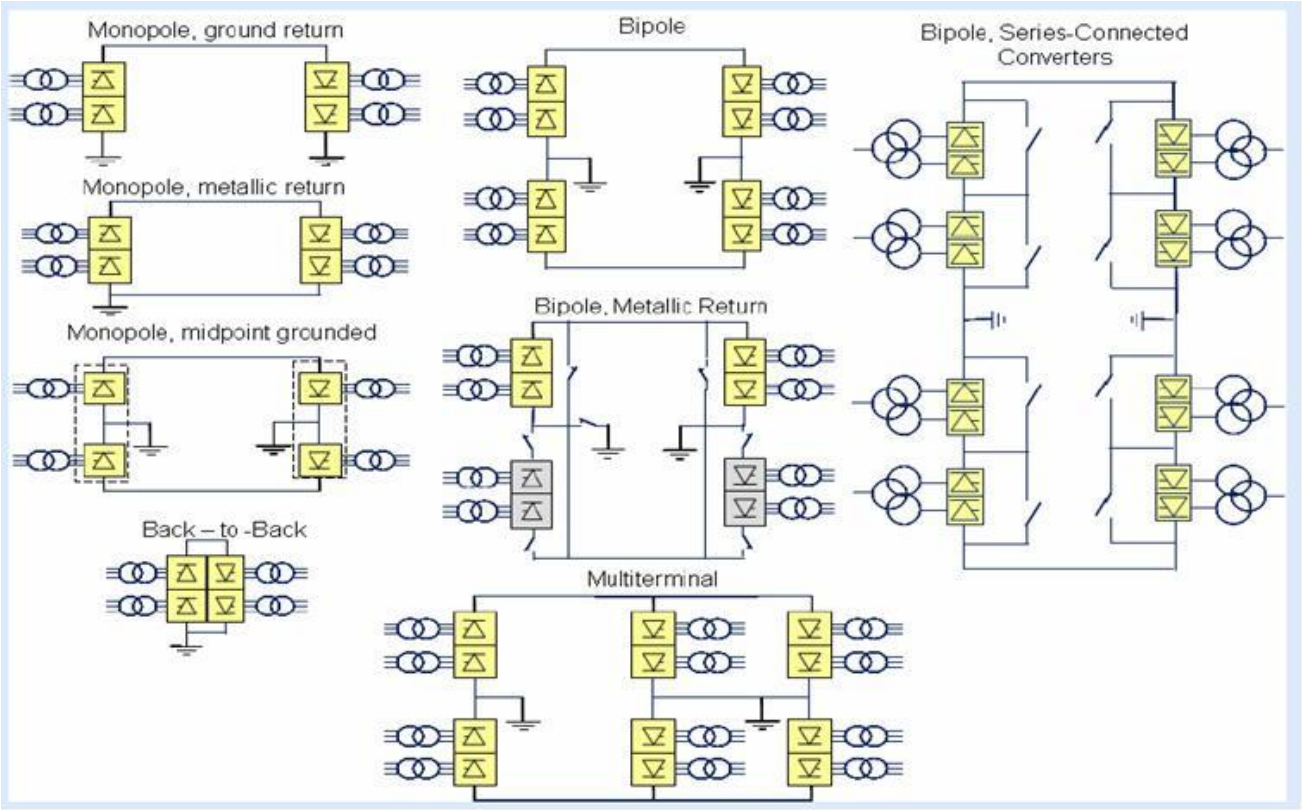

Figure 2.2: Different HVDC schemes

Chapter 3:
Synchronous Machine Modeling

3.1 Introduction

In this chapter we will discuss the modeling and stability analysis of a HVAC link. The most important component of the system is the synchronous generator with its associated controls – excitation and prime mover. The dynamics of a synchronous generator is illustrated by taking up the example of a single machine connected to an infinite bus (SMIB). Although a power station is consists of more than one generator they all can be represented by one single machine. The accuracy of this kind analysis depends on the system data, type of study considered etc. Analysis of the dynamic behavior of a synchronous machine needs the simplification of the SMIB system.

3.2 Modeling of a SMIB System

3.2.1 System Model

We considered a single machine infinite bus model to serve our purpose. One port of the system is connected to the generator terminals while the other port is connected to an infinite bus. To neglect the transients in the external network the analysis involves low frequency behavior of the system which is an important assumption for the analysis. The system considered is shown in figure 3.1.

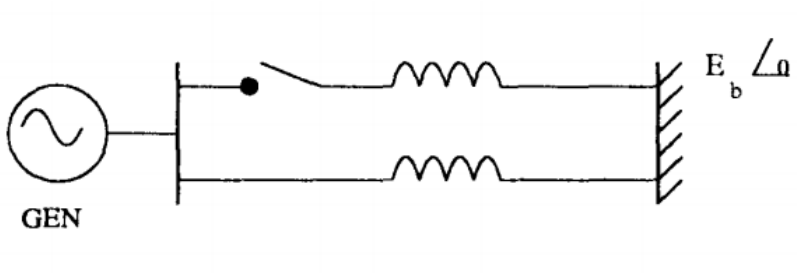

Figure 3.1: Single Machine Infinite Bus System.

3.2.2 Synchronous Machine Model

The synchronous machine considered is shown in Fig. 3.2. This shows a three phase armature windings (a, b and c) on the stator and four windings on the rotor including the field winding 'f'. The amortisseur (or damper) circuits in the salient pole machine or the eddy-current effects in the rotor are represented by a set of coils with constant parameters. Three damper coils, 'h' in the d-axis and g, k on the q-axis are shown in Fig. 3.2. The number of damper coils represented can vary from zero (in the simplest model) to five or more using Jackson-Winchester model. However the most detailed model used extensively in power system dynamic studies is limited to 3 damper coils. (It is also easier to obtain the parameters of this and simpler models). The following assumptions are used in the derivation of the basic equations of the machine.

1. The mmf in the air gap is distributed sinusoidally and the harmonics are neglected.
2. Saliency is restricted to the rotor. The effect of slots in the stator is neglected.
3. Magnetic saturation and hysteresis are ignored.

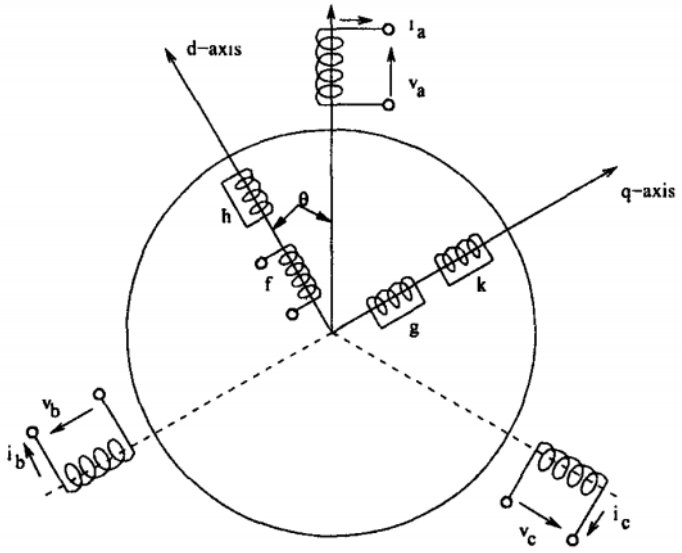

Figure 3.2: Synchronous Machine

The analytical solutions of the equations that we get from the above figure are almost impossible because of the time variant inductance matrix. So it would be advantageous if the time-varying machine equation can be transformed to a time invariant set. This would result in the simplification of the calculations both for steady state and transient conditions.

Parks Transformation transforms time variant AC quantities to time invariant DC quantities. The stator coils 'a', 'b' and 'c' from figure 3.2 are replaced by fictitious 'd', 'q' and '0' coils from Park's transformation. Out of these, '0' coil (in which zero-sequence current io flows) has no coupling with the rotor coils and may be neglected if io = O. Since the (transformed) mutual inductance terms between d, q coils and the rotor coils are constants, it can be interpreted that d and q coils rotate at the same speed as the rotor. Furthermore, as mutual inductances between the d-coil and the rotor coils on the q-axis are zero, it can be assumed that d-coil is aligned with the d-axis. Similarly, it can be assumed that q coil is aligned along with the q-axis. This is shown in Fig. 3.3.

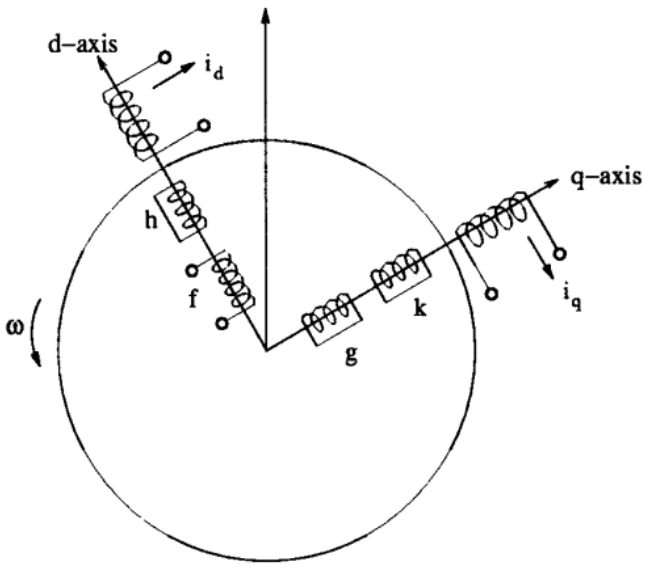

Figure 3.3: Synchronous Machine with rotating armature.

3.3 Initial Condition Calculation

To solve the nonlinear equations of the system we need to calculate the initial conditions based on the system operating point. Phasor diagram of the system described earlier is used to calculate the initial conditions. The phasor diagram is shown in figure 3.4.

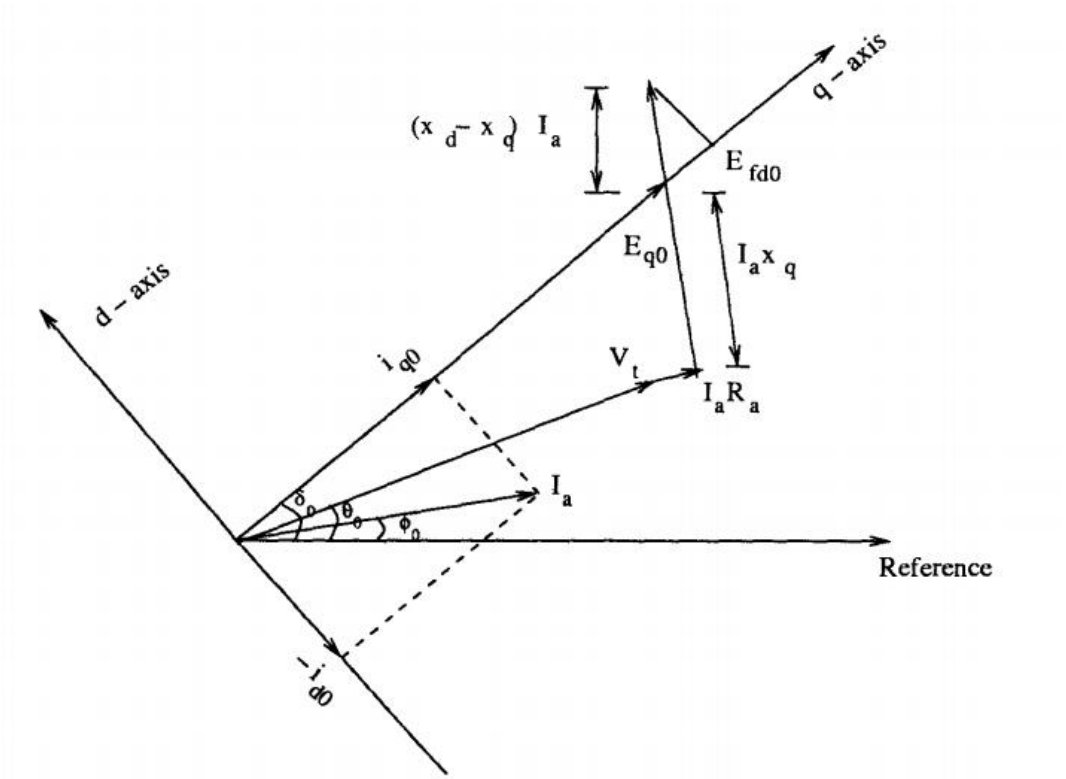

Figure 3.4: Phasor Diagram of the system described earlier.

The procedure for the computation of the initial conditions is given below:

01. Compute I_{ao} from,

$$\hat{I}_{ao} = I_{ao}\angle\phi_o = \frac{P_t - jQ_t}{V_{to}\angle -\theta_o}$$

02. Compute E_{qo} and δ_o from,

$$E_{qo}\angle\delta_o = V_{to}\angle\theta_o + (R_a + jx_q)I_{ao}\angle\phi_o$$

03. Compute,

$$\begin{aligned} i_{do} &= -I_{ao}\sin(\delta_o - \phi_o) \\ i_{qo} &= I_{ao}\cos(\delta_o - \phi_o) \\ v_{do} &= -V_{to}\sin(\delta_o - \theta_o) \\ v_{qo} &= V_{to}\cos(\delta_o - \theta_o) \end{aligned}$$

04. Compute,

$$
\begin{aligned}
E_{fdo} &= E_{qo} - (x_d - x_q) i_{do} \\
E'_{qo} &= E_{fdo} + (x_d - x'_d) i_{do} \\
E'_{do} &= -(x_q - x'_q) i_{qo} \\
T_{eo} &= E'_{qo} i_{qo} + E'_{do} i_{do} + (x'_d - x'_q) i_{do} i_{qo} = T_{mo}
\end{aligned}
$$

3.4 Nonlinear Model of a Synchronous Machine

The system equations for a transient stability study are usually nonlinear. Magnetic saturation is either neglected or considered by using saturated values of mutual inductances x_{dc} (or x_{ad}) and x_{aq}. The machine equations are, which denotes the states of the system,

$$
\begin{aligned}
\frac{d\delta}{dt} &= \omega_B (S_m - S_{mo}) \\
\frac{dS_m}{dt} &= \frac{1}{2H} \left[-D(S_m - S_{mo}) + T_m - T_e \right] \\
\frac{dE'_q}{dt} &= \frac{1}{T'_{do}} \left[-E'_q + (x_d - x'_d) i_d + E_{fd} \right] \\
\frac{dE'_d}{dt} &= \frac{1}{T'_{qo}} \left[-E'_d - (x_q - x'_q) i_q \right]
\end{aligned}
$$

The electrical torque T_e is expressed in terms of the state variables E_d' and E_q' and non-state variables i_d and i_q.

$$
T_e = E'_d i_d + E'_q i_q + (x'_d - x'_q) i_d i_q
$$

To guarantee superposition and homogeneity simultaneously we need to convert the nonlinear equations into linear equation. The knowledge of linearity will also help to design the controller. To convert the nonlinear equation Taylor series is used which is,

$$
f(x) - f(x_0) \approx \left. \frac{df}{dx} \right|_{x=x_0} (x - x_0)
$$

3.5 Linear Model of a Synchronous Machine

By linearizing the nonlinear differential equations, the linearized model of the system is developed. The state space model has been used to study the system dynamic behavior described by the linear differential equations. The techniques of linear system analysis are used to study dynamic behavior of the system. The most common method of studying power system stability is to simulate each component by its transfer function. The various transfer function blocks are connected to represent the system under study. The system performance may then be analyzed by such methods as root-locus plots. Frequency domain analysis (Nyquist criteria), and Routh's criterion. The above methods have been frequently used in studies pertaining to small systems or a small number of machines. For larger systems the state-space model has been used more frequently in connection with system studies described by linear differential equations. Stability characteristics may be determined by examining the eigenvalues of the A matrix, where A is defined by the equation

$$\dot{x} = [A]x + [B](\Delta V_{ref} + \Delta V_s)$$

$$x^t = [\Delta\delta \;\; \Delta S_m \;\; \Delta E'_q \;\; \Delta E_{fd}]$$

$$[A] = \begin{bmatrix} 0 & \omega_B & 0 & 0 \\ -\frac{K_1}{2H} & -\frac{D}{2H} & -\frac{K_2}{2H} & 0 \\ -\frac{K_4}{T'_{do}} & 0 & -\frac{1}{T'_{do}K_3} & \frac{1}{T'_{do}} \\ -\frac{K_E K_5}{T_E} & 0 & -\frac{K_E K_6}{T_E} & -\frac{1}{T_E} \end{bmatrix}$$

$$[B]^t = \begin{bmatrix} 0 & 0 & 0 & \frac{K_E}{T_E} \end{bmatrix}$$

Where x is an n vector denoting the states of the system and A is a coefficient matrix. The system inputs are represented by the vector (ΔV_{ref}+ ΔV_s), and these inputs are related mathematically to differential equations by an nX matrix B. This description has the advantage that A may be time varying and (ΔV_{ref}+ ΔV_s), may be used to represent several inputs if necessary.

$$\Delta\delta = \frac{\omega_B}{s}\Delta S_m = \frac{\omega_B}{s}\Delta\bar{\omega}$$

$$\Delta S_m = \frac{1}{2Hs}\left[\Delta T_m - \Delta T_e - D\Delta S_m\right]$$

$$T'_{do}\frac{d\Delta E'_q}{dt} = \Delta E_{fd} - \Delta E'_q + (x_d - x'_d)(C_1\Delta\delta + C_2\Delta E'_q)$$

Where

$$\Delta T_e = K_1\Delta\delta + K_2\Delta E'_q$$

$$(1 + sT'_{do}K_3)\Delta E'_q = K_3\Delta E_{fd} - K_3K_4\Delta\delta$$

$$\Delta V_t = K_5\Delta\delta + K_6\Delta E'_q$$

Let us consider the armature resistance are neglected, this refers to a lossless stator side. Using the above equations the block diagram of the excitation system is shown in Fig.3.5. The coefficients Kl to K6 are termed as Heffron-Phillips constants. They are dependent on the machine parameters and the operating conditions. Generally Kl, K2, K3 and K6 are positive. K4 is also mostly positive except for cases when Re is high. Ks can be either positive or negative. Ks are positive for low to medium external impedances (Re + jXe) and low to medium loadings. Ks are usually negative for moderate to high external impedances and heavy loadings. The expressions of constants K1-K6 are following,

$$\begin{aligned}
K_1 &= \frac{E_b E_{qo}\cos\delta_o}{(x_e + x_q)} + \frac{(x_q - x'_d)}{(x_e + x'_d)}E_b i_{qo}\sin\delta_o \\
K_2 &= \frac{(x_e + x_q)}{(x_e + x'_d)}i_{qo} = \frac{E_b\sin\delta_o}{(x_e + x'_d)} \\
K_3 &= \frac{(x_e + x'_d)}{(x_d + x_e)} \\
K_4 &= \frac{(x_d - x'_d)}{(x'_d + x_e)}E_b\sin\delta_o \\
K_5 &= \frac{-x_q v_{do}E_b\cos\delta_o}{(x_e + x_q)V_{to}} - \frac{x'_d v_{qo}E_b\sin\delta_o}{(x_e + x'_d)V_{to}} \\
K_6 &= \frac{x_e}{(x_e + x'_d)}.\left(\frac{v_{qo}}{V_{to}}\right)
\end{aligned}$$

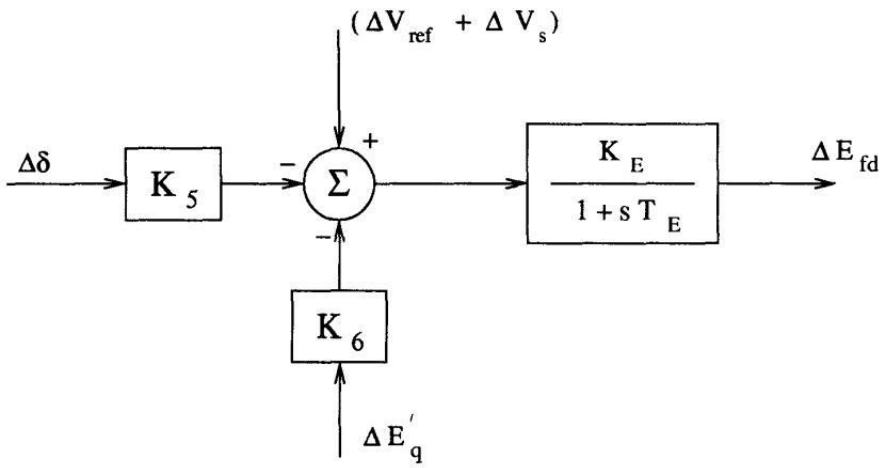

Figure 3.5: Excitation System Block Diagram

The system block diagram is obtained by combining the rotor swing equations, flux decay and excitation system. The overall block diagram is shown in Fig. 3.6. Here the damping term (D) in the swing equations is neglected for convenience. (Actually D is generally small and neglecting it will give slightly pessimistic results).

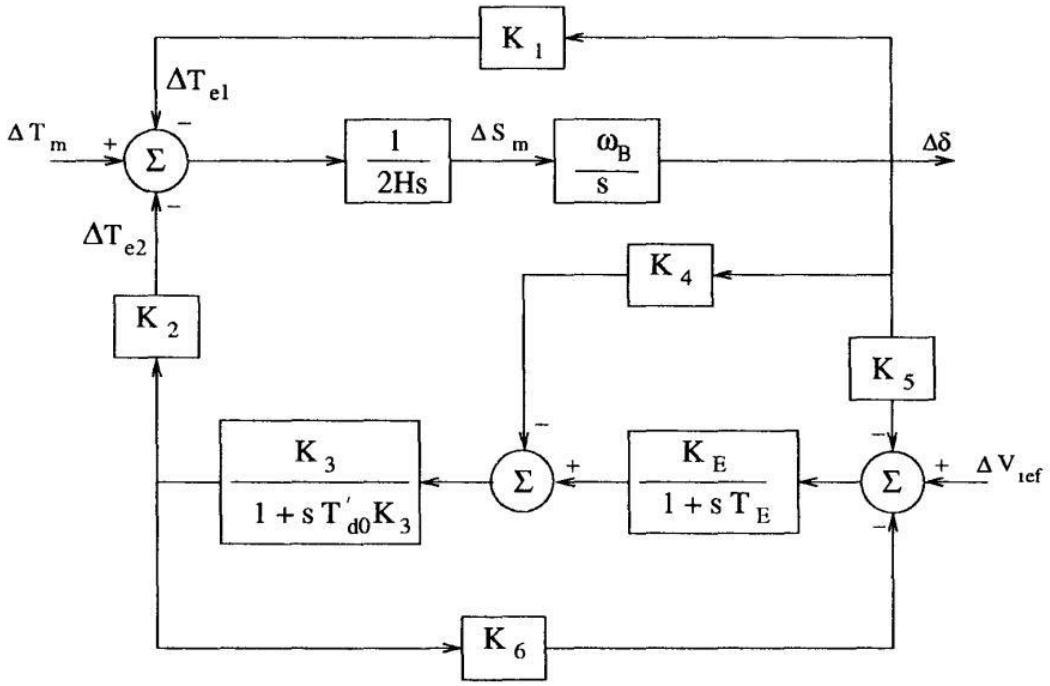

Figure 3.6: Overall System Block diagram

3.6 Automatic Voltage Regulator

The Automatic Voltage Regulator (AVR) maintains a constant or stable output voltage during operation, usually by varying the field voltage. Most AVR work automatically comparing the sensed voltage with the reference setting generator output voltage.

Transient stability is improved by using automatic voltage regulator. In fault condition, field voltage is increased to keep generator voltage constant.

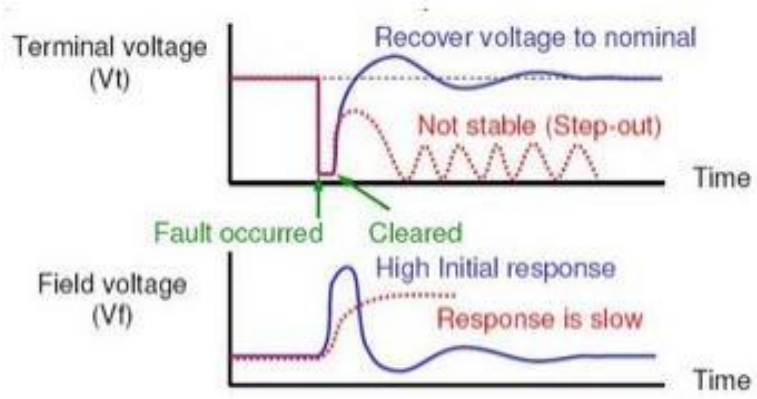

Figure 3.7: Response of AVR.

3.7 MATLAB Codes for Initial Condition Calculation

```
Xd=1.8;
Xq=1.7;
X0d=.17;
X0q=.23;
Pt=1;
Eb=1;
Vt=1;
Xe=.25;
X=asind(Pt*Xe/(Vt*Eb))
Y=asin(Pt*Xe/(Vt*Eb));
Ia=(Vt.*exp(i*Y)-Eb)/(i*Xe)
Eqo=Vt.*exp(i*Y)+i*Xq*Ia
A=angle(Eqo);
B=angledim(A,'radians','degrees');
C=angle(Ia);
D=angledim(C,'radians','degrees');
Ido=-abs(Ia)*sind(B-D)
Iqo=abs(Ia)*cosd(B-D)
Efdo=abs(Eqo)-(Xd-Xq)*Ido
E0qo=Efdo+(Xd-X0d)*Ido
E0do=-(Xq-X0q)*Iqo
Teo=E0qo*Iqo+E0do*Ido+(X0d-X0q)*Ido*Iqo
```

Simulation Result

Simulation has been done for four different cases,

1. Pt=0.9 ; Qt=0.6.
2. Pt=0.9 ; Qt=-.02.
3. Pt=0.3 ; Qt=0.02.
4. Pt=0.3 ; Qt=0.36.

Variables	Case 01	Case 02	Case 03	Case 04
δ	44.10	69.73	30.27	71.38
E'_q	1.11	0.6813	0.9312	0.3893
E'_d	-0.4568	-0.6126	-0.3273	-0.6145
i_d	-0.9221	-0.7813	-0.1536	-0.1535
i_q	0.3597	0.4824	0.2577	0.4838
E_{fd}	2.6787	2.0094	1.1923	0.6503

3.8 MATLAB Codes for Dynamic Behavior of the System without Switching

```
clear all; clc;
xd=1.93;
xq=1.77;
xd0=.23;
xq0=.50;
Pt=.9;
Eb=1;
Vt=0.9804;
xe0=.192;
xe=xe0;
Pm=.9;
H=3.74;
w0=2*pi*60;
w=1;
td0=5.2;
tq0=.81;
X=asind(Pt*xe0/(Vt*Eb));
Y=asin(Pt*xe0/(Vt*Eb));
Ia=(Vt.*exp(1i*Y)-Eb)/(1i*xe0);
Eqo=Vt.*exp(1i*Y)+(1i*xq*Ia);
A=angle(Eqo);
B=angledim(A,'radians','degrees');
C=angle(Ia);
D=angledim(C,'radians','degrees');
Ido=abs(Ia)*sind(B-D);
Iqo=abs(Ia)*cosd(B-D);
Efd0=abs(Eqo)+(xd-xq)*Ido;
E0qo=Efd0-(xd-xd0)*Ido;
E0do=(xq-xq0)*Iqo;

id(1)=Ido;
iq(1)=Iqo;
y1(1)=E0qo;
y2(1)=w;
y3(1)=A;

Ts=.001;
tsim=20;
t=zeros(1,tsim/Ts);
flt_strt=1.0;
for n=1:length(t)

  t(n+1)=t(n)+Ts;

vd(n)=xq*iq(n);
vq(n)=y1(n)-xd0*id(n);
vt(n)=sqrt(vd(n)^2+vq(n)^2);
Pe(n)=vd(n)*id(n)+vq(n)*iq(n);
y1(n+1)=y1(n)+Ts*((1/td0)*(-y1(n)-(xd-xd0)*id(n)+Efd0));
y2(n+1)=y2(n)+Ts*((1/(2*H))*(Pm-Pe(n)));
y3(n+1)=y3(n)+Ts*(w0*(y2(n)-1));
```

```
id(n+1)=(y1(n)-Eb*cos(y3(n)))/(xd0+xe);
iq(n+1)=(Eb*sin(y3(n)))/(xe+xq);
end
subplot(2,1,1);
plot(t(1:end-1),vt)
xlabel('time(t)')
ylabel('terminal voltage ')
title( 'variation of terminal voltage')

subplot(2,1,2);
plot(t,y3)
xlabel('time(t)')
ylabel('rotor angle ')
title( 'swing curve')
```

Simulation Results

(i) For case 01

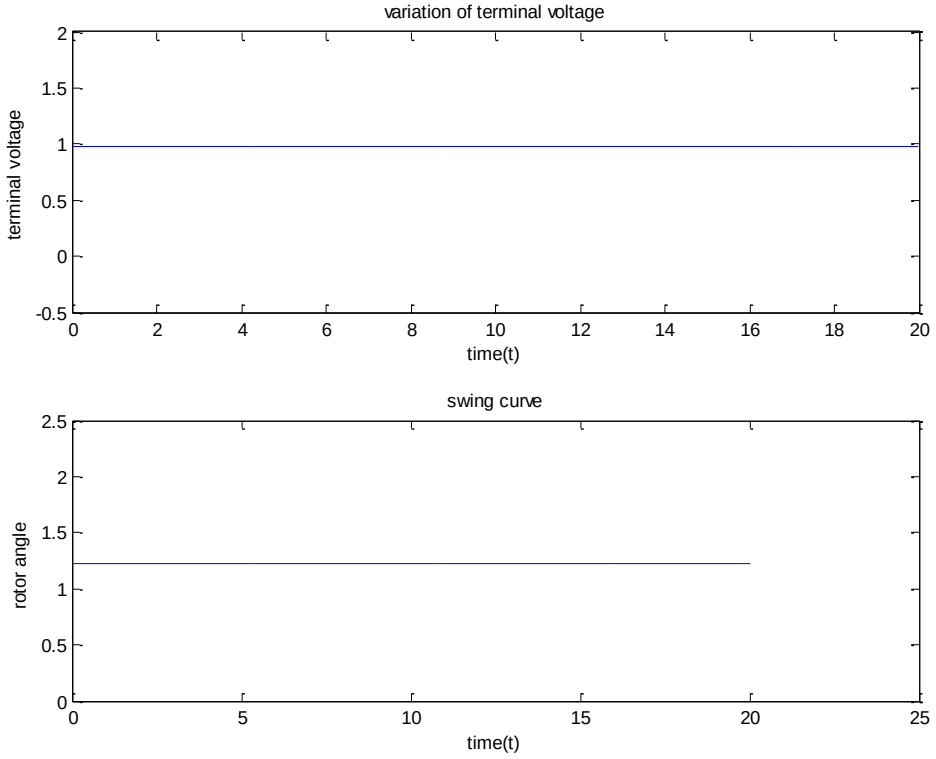

(ii) For case 02

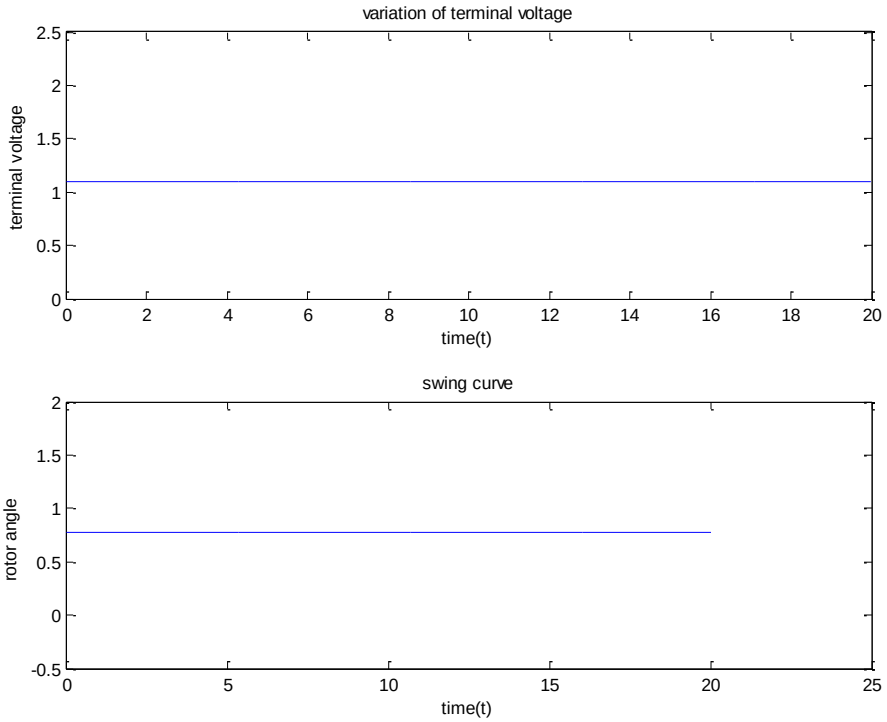

(iii) For case 03

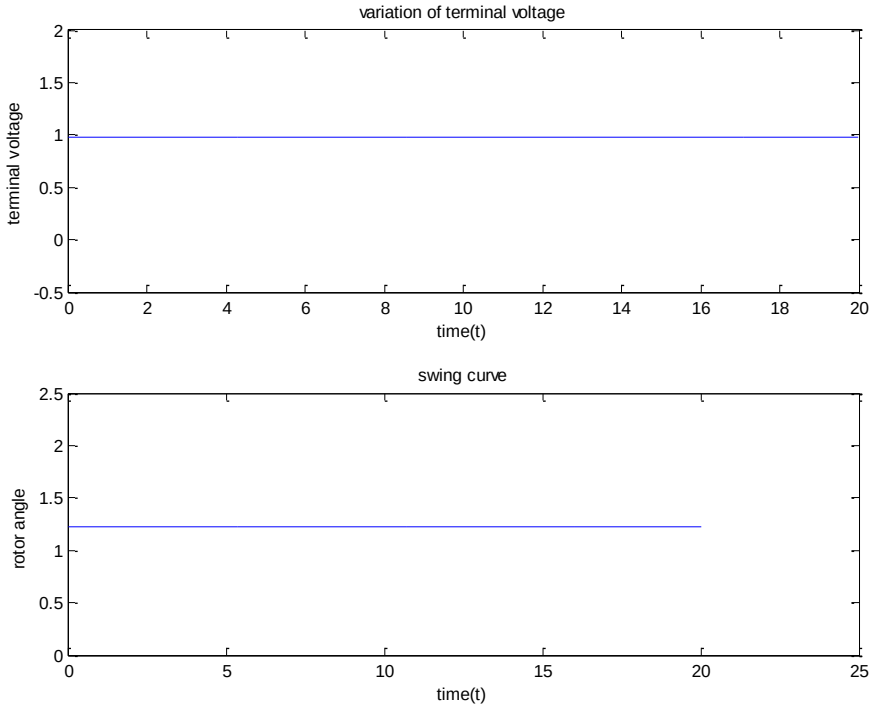

(iv) For case 04

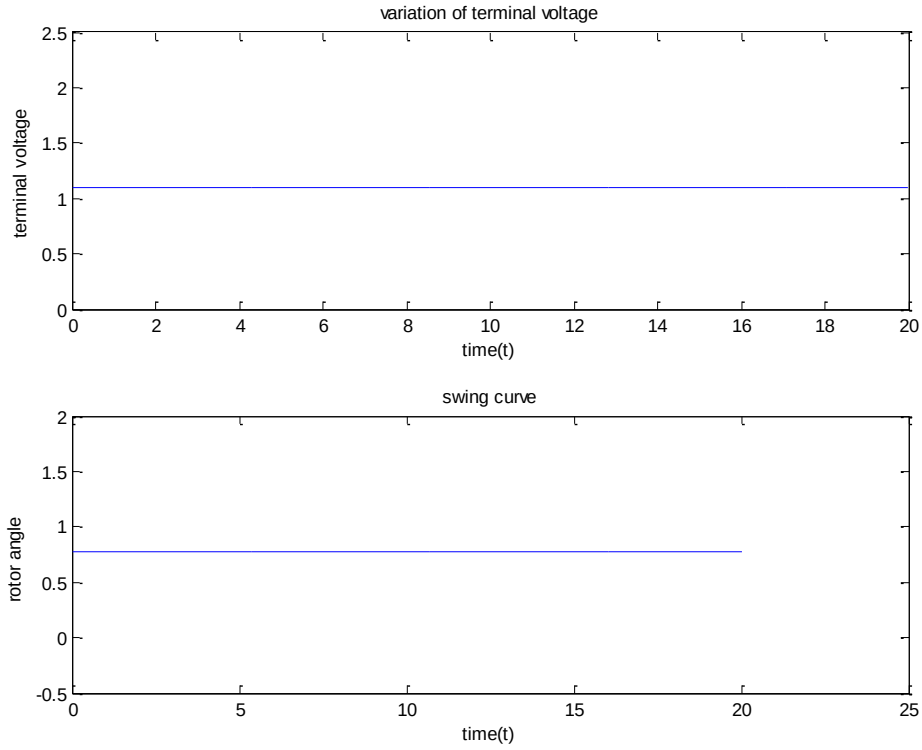

3.9 MATLAB Codes for Dynamic Behavior of the System after Switching

```
clear all; clc;
xd=1.93;
xq=1.77;
xd0=.23;
xq0=.50;
Pt=.9;
Eb=1;
Vt=0.9804;
xe0=.192;
xe=xe0;
Pm=.9;
H=3.74;
w0=2*pi*60;
w=1;
td0=5.2;
tq0=.81;
X=asind(Pt*xe0/(Vt*Eb));
Y=asin(Pt*xe0/(Vt*Eb));
Ia=(Vt.*exp(1i*Y)-Eb)/(1i*xe0);
Eqo=Vt.*exp(1i*Y)+(1i*xq*Ia);
```

```
A=angle(Eqo);
B=angledim(A,'radians','degrees');
C=angle(Ia);
D=angledim(C,'radians','degrees');
Ido=abs(Ia)*sind(B-D);
Iqo=abs(Ia)*cosd(B-D);
Efd0=abs(Eqo)+(xd-xq)*Ido;
E0qo=Efd0-(xd-xd0)*Ido;
E0do=(xq-xq0)*Iqo;

id(1)=Ido;
iq(1)=Iqo;
y1(1)=E0qo;
y2(1)=w;
y3(1)=A;

Ts=.001;
tsim=20;
t=zeros(1,tsim/Ts);
flt_strt=1.0;
for n=1:length(t)
    t(n+1)=t(n)+Ts;

vd(n)=xq*iq(n);
vq(n)=y1(n)-xd0*id(n);
vt(n)=sqrt(vd(n)^2+vq(n)^2);
Pe(n)=vd(n)*id(n)+vq(n)*iq(n);
y1(n+1)=y1(n)+Ts*((1/td0)*(-y1(n)-(xd-xd0)*id(n)+Efd0));
y2(n+1)=y2(n)+Ts*((1/(2*H))*(Pm-Pe(n)));
y3(n+1)=y3(n)+Ts*(w0*(y2(n)-1));

 if n<flt_strt/Ts
        xe=.192;
    else
        xe=.055;
 end

id(n+1)=(y1(n)-Eb*cos(y3(n)))/(xd0+xe);
iq(n+1)=(Eb*sin(y3(n)))/(xe+xq);
end
subplot(2,1,1);
plot(t(1:end-1),vt)
xlabel('time(t)')
ylabel('terminal voltage ')
title( 'variation of terminal voltage')
subplot(2,1,2);
plot(t,y3)
xlabel('time(t)')
ylabel('rotor angle ')
title( 'swing curve')
```

Simulation Result

(i) For case 01

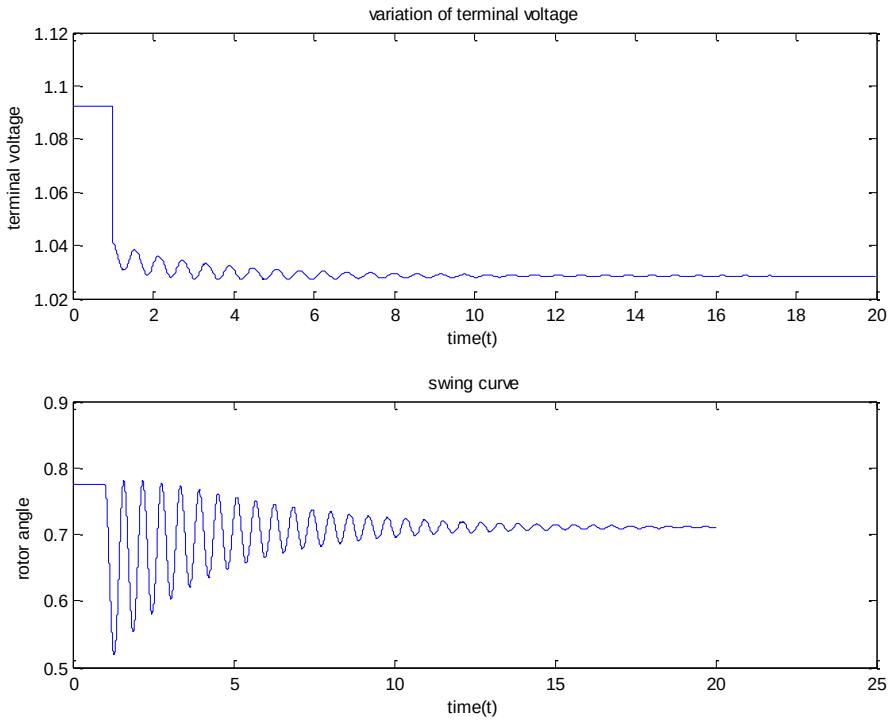

(ii) For case 02

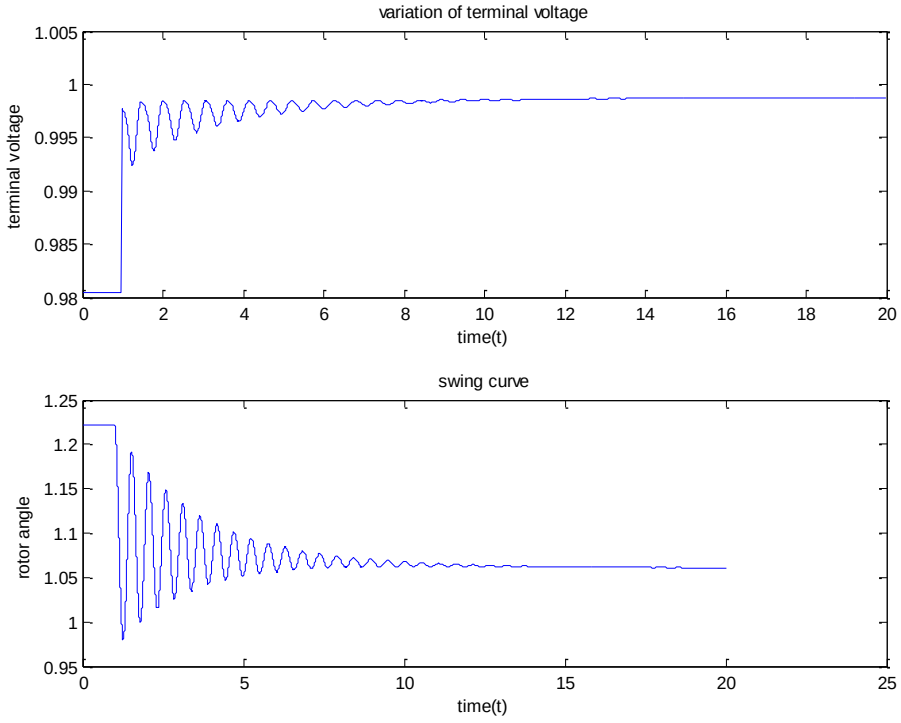

(iii) For case 03

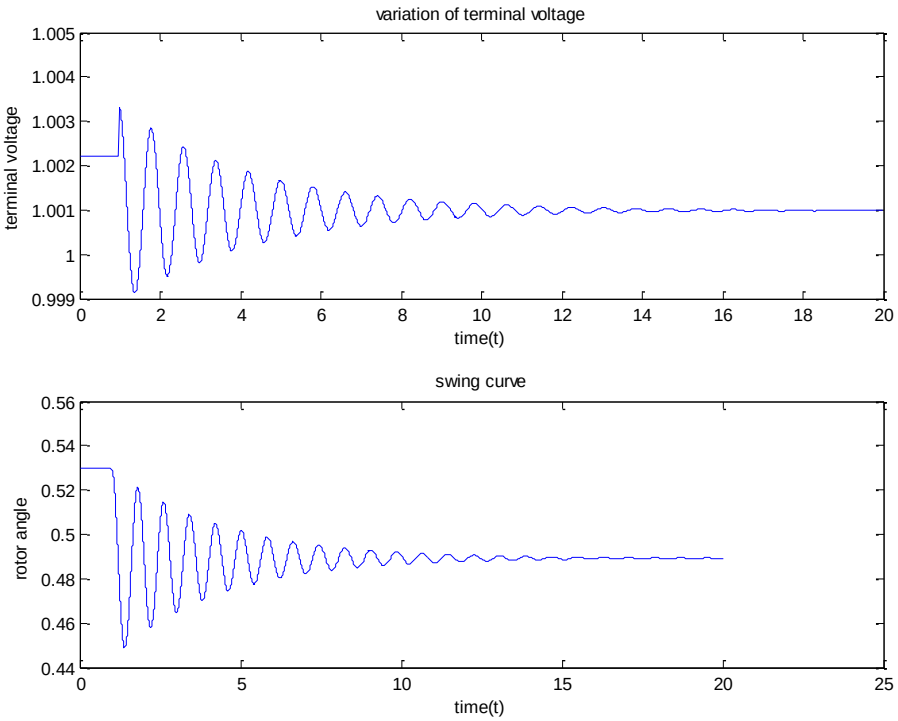

(iv) For case 04

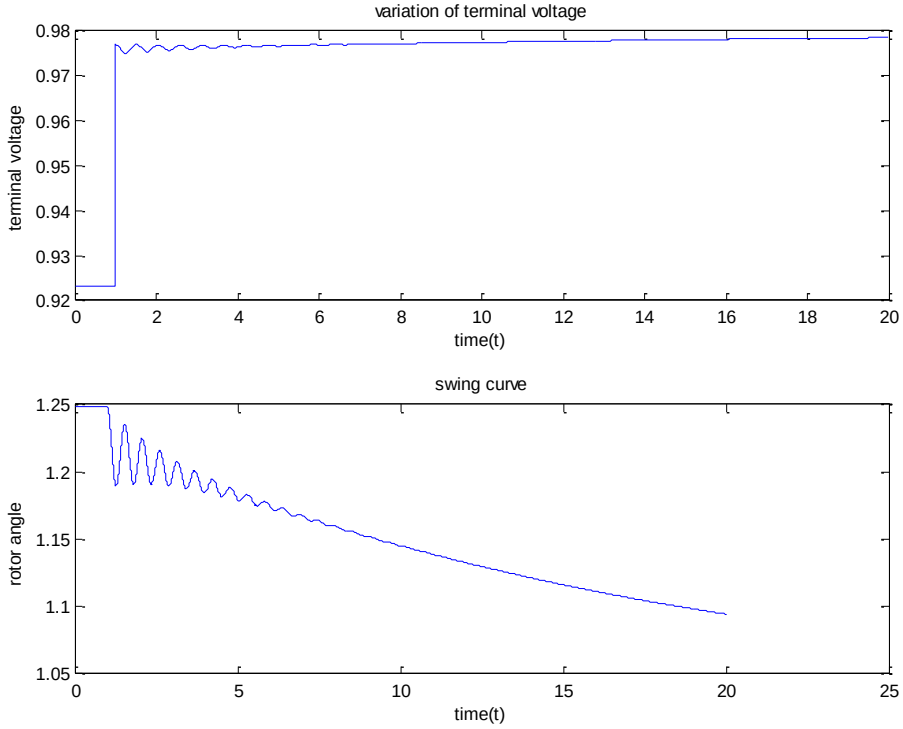

3.10 MATLAB Codes for Calculation of Phillips Heffron Constants k_1 to k_6

```
clear all; clc;
xd=1.6;
xq=1.55;
xd0=.32;
Pt=.5;
Eb=1;
Vt=1;
xe0=.4;
xe=xe0;
Pm=Pt;
H=5;
w0=2*pi*60;
w=1;
td0=6;
X=asind(Pt*xe0/(Vt.*Eb));
Y=asin(Pt*xe0/(Vt.*Eb));
Vt0=Vt.*exp(1i*Y);
Ia=(Vt.*exp(1i*Y)-Eb)/(1i*xe0);
Eq=Vt.*exp(1i*Y)+(1i*xq*Ia);
Eq0=abs(Eq);
A=angle(Eq);
B=angledim(A,'radians','degrees');
C=angle(Ia);
D=angledim(C,'radians','degrees');
Ido=abs(Ia)*sind(B-D);
Iqo=abs(Ia)*cosd(B-D);
Efd0=abs(Eq)+(xd-xq)*Ido;
Eqpo=Efd0-(xd-xd0)*Ido;

Vdo=xq*Iqo;
Vqo=abs(Eqpo)-(xd0*Ido);
Teo=Vdo*Ido+Vqo*Iqo;

% Heffron_Phillips constant_
R=0;
Z=(xd0+xe)*(xq+xe)+R^2;
c1=((xq+xe)*Eb*sin(A)-R*Eb*cos(A))/Z;
c2=(xq+xe)/Z;
c3=((xd0+xe)*Eb*cos(A)+R*Eb*sin(A))/Z;
c4=R/Z;

K1=(Eq0)*c3+Iqo*c1*(xq-xd0)
K2=Eqpo*c4+Iqo+Iqo*(xq-xd0)*c2
K3=1/(1+c2*(xd-xd0))
K4=c1*(xd-xd0)
K5=((Vdo/abs(Vt0))*xq*c3)-((Vqo/abs(Vt0))*xd0*c1)
K6=((Vdo/abs(Vt0))*xq*c4)+((Vqo/abs(Vt0))*(1-xd0*c2))
```

Simulation Results

K_1= 0.9346

K_2=1.0198

K_3=.3600

K_4=1.3053

K_5=.0500

K_6=.4511

3.11 MATLAB Codes for Variation of Linearization Constants with the Variation of x_e

```
clear all; clc;
 % initail condition calculation
xd=1.6;
xq=1.55;
xd0=.32;
Pt=.5;
Eb=1;
Vt=1;
Pm=Pt;
H=5;
w0=2*pi*60;
w=1;
td0=6;
for xe=.1:.001:1

X=asind(Pt*xe/(Vt.*Eb));
Y=asin(Pt*xe/(Vt.*Eb));
Vt0=Vt.*exp(1i*Y);
Ia=(Vt.*exp(1i*Y)-Eb)/(1i*xe);
Eq=Vt.*exp(1i*Y)+(1i*xq*Ia);
Eq0=abs(Eq);
A=angle(Eq);
B=angledim(A,'radians','degrees');
C=angle(Ia);
D=angledim(C,'radians','degrees');
Ido=abs(Ia)*sind(B-D);
Iqo=abs(Ia)*cosd(B-D);
Efd0=abs(Eq)+(xd-xq)*Ido;
Eqpo=Efd0-(xd-xd0)*Ido;
Vdo=xq*Iqo;
Vqo=abs(Eqpo)-(xd0*Ido);
Teo=Vdo*Ido+Vqo*Iqo;
% Heffron_Phillips constant_
R=0;
Z=(xd0+xe)*(xq+xe)+R^2;
c1=((xq+xe)*Eb*sin(A)-R*Eb*cos(A))/Z;
```

```
c2=(xq+xe)/Z;
c3=((xd0+xe)*Eb*cos(A)+R*Eb*sin(A))/Z;
c4=R/Z;
K1=(Eq0)*c3+Iqo*c1*(xq-xd0);
K2=Eqpo*c4+Iqo+Iqo*(xq-xd0)*c2;
K3=1/(1+c2*(xd-xd0));
K4=c1*(xd-xd0);
K5=((Vdo/abs(Vt0))*xq*c3)-((Vqo/abs(Vt0))*xd0*c1);
K6=((Vdo/abs(Vt0))*xq*c4)+((Vqo/abs(Vt0))*(1-xd0*c2));
M=K1-(K2*K3*K4);
subplot(3,1,1)
plot(xe,K1,'--')
hold all
xlabel('xe')
ylabel('K1')
subplot(3,1,2)
plot(xe,M,'--')
hold all
xlabel('xe')
ylabel('K1-K2K3K4')
subplot(3,1,3)
plot(xe,K5)
hold all
xlabel('xe')
ylabel('K5')
end
```

Simulation Results

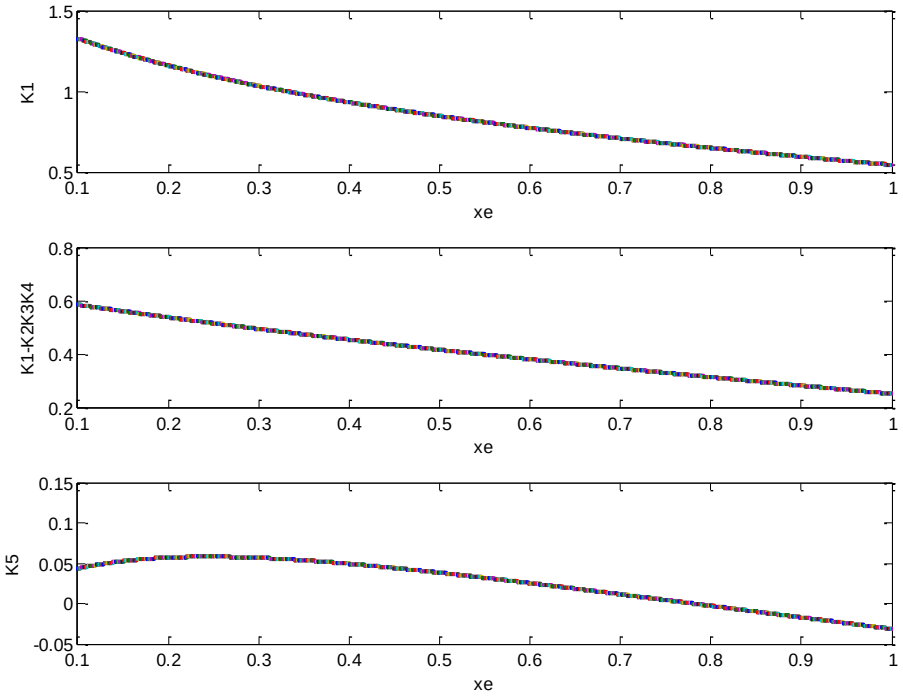

3.12 MATLAB Codes for Variation of Parameters with the Variation of P_G

```
clear all; clc;
% initail condition calculation
xd=1.6;
xq=1.55;
xd0=.32;
Pt=.5;
Eb=1;
Vt=1;
xe0=.4;
xe=xe0;
Pm=Pt;
H=5;
w0=2*pi*60;
w=1;
td0=6;
for Pt=.5:.001:1.5

X=asind(Pt*xe0/(Vt.*Eb));
Y=asin(Pt*xe0/(Vt.*Eb));
Vt0=Vt.*exp(1i*Y);
Ia=(Vt.*exp(1i*Y)-Eb)/(1i*xe0);
Eq=Vt.*exp(1i*Y)+(1i*xq*Ia);
Eq0=abs(Eq);
A=angle(Eq);
B=angledim(A,'radians','degrees');
C=angle(Ia);
D=angledim(C,'radians','degrees');
Ido=abs(Ia)*sind(B-D);
Iqo=abs(Ia)*cosd(B-D);
Efd0=abs(Eq)+(xd-xq)*Ido;
Eqpo=Efd0-(xd-xd0)*Ido;
Vdo=xq*Iqo;
Vqo=abs(Eqpo)-(xd0*Ido);
Teo=Vdo*Ido+Vqo*Iqo;
 % Heffron_Phillips constant_
R=0;
Z=(xd0+xe)*(xq+xe)+R^2;
c1=((xq+xe)*Eb*sin(A)-R*Eb*cos(A))/Z;
c2=(xq+xe)/Z;
c3=((xd0+xe)*Eb*cos(A)+R*Eb*sin(A))/Z;
c4=R/Z;



K1=(Eq0)*c3+Iqo*c1*(xq-xd0);
K2=Eqpo*c4+Iqo+Iqo*(xq-xd0)*c2;
K3=1/(1+c2*(xd-xd0));
K4=c1*(xd-xd0);
K5=((Vdo/abs(Vt0))*xq*c3)-((Vqo/abs(Vt0))*xd0*c1);
K6=((Vdo/abs(Vt0))*xq*c4)+((Vqo/abs(Vt0))*(1-xd0*c2));
M=K1-(K2*K3*K4);
```

```
% ploting
subplot(3,1,1)
plot(Pt,K1,'--')
hold all
xlabel('Pg')
ylabel('K1')
subplot(3,1,2)
plot(Pt,M,'--')
hold all
xlabel('Pg')
ylabel('K1-K2K3K4')
subplot(3,1,3)
plot(Pt,K5)
hold all
xlabel('Pg')
ylabel('K5')
end
```

Simulation Results

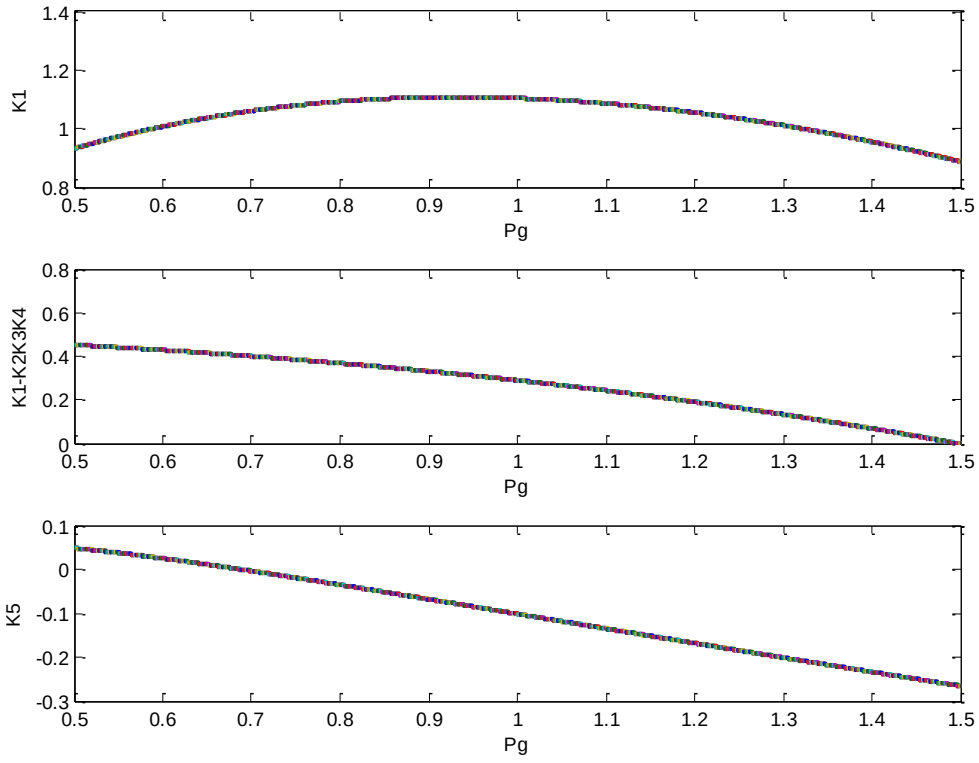

3.13 MATLAB Codes for Calculation of Eigenvalues of System Matrix [A]

```
clear all; clc;

% initail condition calculation
xd=1.6;
xq=1.55;
xd0=.32;
Pt=1;
Eb=1;
Vt=1;
xe0=.4;
xe=xe0;
Pm=Pt;
H=5;
w0=2*pi*60;
w=1;
td0=6;
Te=.05;
Ke=200;
X=asind(Pt*xe0/(Vt.*Eb));
Y=asin(Pt*xe0/(Vt.*Eb));
Vt0=Vt.*exp(1i*Y);
Ia=(Vt.*exp(1i*Y)-Eb)/(1i*xe0);
Eq=Vt.*exp(1i*Y)+(1i*xq*Ia);
Eq0=abs(Eq);
A=angle(Eq);
B=angledim(A,'radians','degrees');
C=angle(Ia);
D=angledim(C,'radians','degrees');
Ido=abs(Ia)*sind(B-D);
Iqo=abs(Ia)*cosd(B-D);
Efd0=abs(Eq)+(xd-xq)*Ido;
Eqpo=Efd0-(xd-xd0)*Ido;
Vdo=xq*Iqo;
Vqo=abs(Eqpo)-(xd0*Ido);
Teo=Vdo*Ido+Vqo*Iqo;
 % Heffron_Phillips constant_
R=0;
Z=(xd0+xe)*(xq+xe)+R^2;
c1=((xq+xe)*Eb*sin(A)-R*Eb*cos(A))/Z;
c2=(xq+xe)/Z;
c3=((xd0+xe)*Eb*cos(A)+R*Eb*sin(A))/Z;
c4=R/Z;
 K1=(Eq0)*c3+Iqo*c1*(xq-xd0);
K2=Eqpo*c4+Iqo+Iqo*(xq-xd0)*c2;
K3=1/(1+c2*(xd-xd0));
K4=c1*(xd-xd0);
K5=((Vdo/abs(Vt0))*xq*c3)-((Vqo/abs(Vt0))*xd0*c1);
K6=((Vdo/abs(Vt0))*xq*c4)+((Vqo/abs(Vt0))*(1-xd0*c2));
 %eiganvalue calculation
E=[0 w0 0;(-K1/(2*H)) 0 (-K2/(2*H));(-K4/td0) 0 (-1/(td0*K3))];
R=eig(E)
plot(real(R(1)),imag(R(1)),'*')
```

```
hold all
F=[0 w0 0 0;(-K1/(2*H)) 0 (-K2/(2*H)) 0;(-K4/td0) 0 (-1/(td0*K3)) (1/td0);(-
Ke*K5/Te) 0 (-Ke*K6/Te) (-1/Te)];
Q=eig(F)
```

Simulation Results

Eigen Value Analysis

P_g = 1.0

Without AVR,

-0.1702 + 6.4518i
-0.1702 - 6.4518i
-0.1225

With AVR,

-10.7405 +12.1037i
-10.7405 -12.1037i
0.5091 + 7.1561i
0.5091 - 7.1561i

P_g =0.5

Without AVR,

-0.1185 + 5.9301i
-0.1185 - 5.9301i
-0.2259

With AVR,

-10.0803 +14.3810i
-10.0803 -14.3810i
-0.1512 + 5.5406i
-0.1512 - 5.5406i

3.14 MATLAB Codes for Plotting Eigenvalue Loci for Variation in P_g (without AVR)

```
clear all; clc;
% initail condition calculation
xd=1.6;
xq=1.55;
xd0=.32;
Pt=1;
Eb=1;
Vt=1;
xe0=.4;
xe=xe0;
Pm=Pt;
H=5;
w0=2*pi*60;
w=1;
td0=6;
Te=.05;
Ke=200;

for Pt=0.5:.01:1.7;
X=asind(Pt*xe/(Vt.*Eb));
Y=asin(Pt*xe/(Vt.*Eb));
Vt0=Vt.*exp(1i*Y);
Ia=(Vt.*exp(1i*Y)-Eb)/(1i*xe);
Eq=Vt.*exp(1i*Y)+(1i*xq*Ia);
Eq0=abs(Eq);
```

```
A=angle(Eq);
B=angledim(A,'radians','degrees');
C=angle(Ia);
D=angledim(C,'radians','degrees');
Ido=abs(Ia)*sind(B-D);
Iqo=abs(Ia)*cosd(B-D);
Efd0=abs(Eq)+(xd-xq)*Ido;
Eqpo=Efd0-(xd-xd0)*Ido;
Vdo=xq*Iqo;
Vqo=abs(Eqpo)-(xd0*Ido);
Teo=Vdo*Ido+Vqo*Iqo;
% Heffron_Phillips constant_
R=0;
Z=(xd0+xe)*(xq+xe)+R^2;
c1=((xq+xe)*Eb*sin(A)-R*Eb*cos(A))/Z;
c2=(xq+xe)/Z;
c3=((xd0+xe)*Eb*cos(A)+R*Eb*sin(A))/Z;
c4=R/Z;
K1=(Eq0)*c3+Iqo*c1*(xq-xd0);
K2=Eqpo*c4+Iqo+Iqo*(xq-xd0)*c2;
K3=1/(1+c2*(xd-xd0));
K4=c1*(xd-xd0);
K5=((Vdo/abs(Vt0))*xq*c3)-((Vqo/abs(Vt0))*xd0*c1);
K6=((Vdo/abs(Vt0))*xq*c4)+((Vqo/abs(Vt0))*(1-xd0*c2));
%eiganvalue calculation
E=[0 w0 0;(-K1/(2*H)) 0 (-K2/(2*H));(-K4/td0) 0 (-1/(td0*K3))];
R=eig(E)
plot(real(R(1)),imag(R(1)),'*')
hold all
F=[0 w0 0 0;(-K1/(2*H)) 0 (-K2/(2*H)) 0;(-K4/td0) 0 (-1/(td0*K3)) (1/td0);(-
Ke*K5/Te) 0 (-Ke*K6/Te) (-1/Te)];
Q=eig(F)
 end
```

Simulation Result

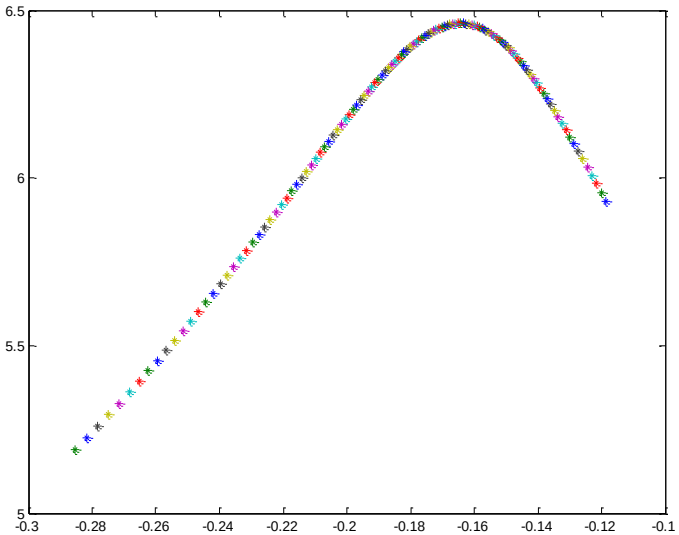

3.15 MATLAB Codes for Plotting Eigenvalue Loci for Variation in X_E (without AVR)

```
clear all; clc;

% initail condition calculation
xd=1.6;
xq=1.55;
xd0=.32;
Pt=1;
Eb=1;
Vt=1;
xe0=.4;
Pm=Pt;
H=5;
w0=2*pi*60;
w=1;
td0=6;
Te=.05;
Ke=200;
for xe=0.1:.01:1;
X=asind(Pt*xe/(Vt.*Eb));
Y=asin(Pt*xe/(Vt.*Eb));
Vt0=Vt.*exp(1i*Y);
Ia=(Vt.*exp(1i*Y)-Eb)/(1i*xe);
Eq=Vt.*exp(1i*Y)+(1i*xq*Ia);
Eq0=abs(Eq);
A=angle(Eq);
B=angledim(A,'radians','degrees');
C=angle(Ia);
D=angledim(C,'radians','degrees');
Ido=abs(Ia)*sind(B-D);
Iqo=abs(Ia)*cosd(B-D);
Efd0=abs(Eq)+(xd-xq)*Ido;
Eqpo=Efd0-(xd-xd0)*Ido;
Vdo=xq*Iqo;
Vqo=abs(Eqpo)-(xd0*Ido);
Teo=Vdo*Ido+Vqo*Iqo;

% Heffron_Phillips constant_
R=0;
Z=(xd0+xe)*(xq+xe)+R^2;
c1=((xq+xe)*Eb*sin(A)-R*Eb*cos(A))/Z;
c2=(xq+xe)/Z;
c3=((xd0+xe)*Eb*cos(A)+R*Eb*sin(A))/Z;
c4=R/Z;

K1=(Eq0)*c3+Iqo*c1*(xq-xd0);
K2=Eqpo*c4+Iqo+Iqo*(xq-xd0)*c2;
K3=1/(1+c2*(xd-xd0));
K4=c1*(xd-xd0);
K5=((Vdo/abs(Vt0))*xq*c3)-((Vqo/abs(Vt0))*xd0*c1);
K6=((Vdo/abs(Vt0))*xq*c4)+((Vqo/abs(Vt0))*(1-xd0*c2));

%eiganvalue calculation
E=[0 w0 0;(-K1/(2*H)) 0 (-K2/(2*H));(-K4/td0) 0 (-1/(td0*K3))];
```

```
R=eig(E)
plot(real(R(1)),imag(R(1)),'*')
hold all
F=[0 w0 0 0;(-K1/(2*H)) 0 (-K2/(2*H)) 0;(-K4/td0) 0 (-1/(td0*K3)) (1/td0);(-
Ke*K5/Te) 0 (-Ke*K6/Te) (-1/Te)];
Q=eig(F)
end
```

Simulation Result

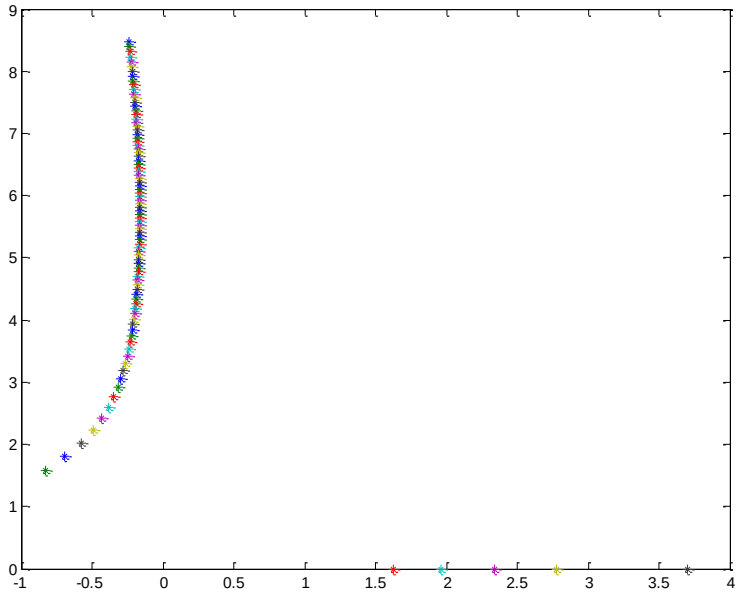

3.16 Discussion

Condition for stability:

AVR is not considered

$K_1 > 0$,

$K_1 - K_2K_3K_4 > 0$

AVR is considered, **$K_E < K_4 / -K_5$**

Observing simulation result from article 3.11 and 3.12 we can see that for certain range of values of P_g and X_e the above conditions are satisfied. And the system remains stable.

From the simulation result of article 3.13 we can see that for P_g = 1 we get some positive eigenvalues which means our system is unstable for that certain value of P_g.

Chapter 4:
Modeling and Stability Analysis of VSC-HVDC System

4.1. Introduction

HVDC systems interconnect large power systems and offer economic benefits. The usage of these systems includes for example non-synchronous interconnection, control of power flow, and modulation to increase stability limits. The transient stability of the AC systems in a composite AC–DC system can be improved by taking advantage of the fast controllability of HVDC converters [5]. Therefore, it is better to construct HVDC links close to HVAC lines.

The VSC HVDC system is the modern HVDC technology. It consists of two VSCs, one of them operates as a rectifier and the other one acts as an inverter. The two converters are connected through a DC line. Its main function is to transmit a constant DC power from the rectifier station to the inverter station, with high controllability [5].

In this chapter, a HVAC system in a parallel VSC HVDC system has been modeled as nonlinear state space equations and then these equations have been linearized around operating point in order to analyze the small -signal stability of the system and to design phase compensator. These phase compensator parameters are set for particular operating point, therefore the controller parameters tune cannot guarantee its performance in another operating point. Also, it may not be able to suppress oscillations resulted from severe disturbances, especially those three-phase faults which may occur at the generator terminals.

4.2. Description of the case study system

Figure 4.1 shows a SMIB system equipped with a HVDC. The synchronous generator is delivering power to the infinite-bus through a double circuit transmission line. The HVDC link is installed in one of the two parallel transmission lines. This configuration, comprising two parallel transmission lines, permits the control of real and reactive power flow through a line. The HVDC consists of two coupling transformer, two three- phase IGBT based voltage source converters (VSCs). These two IGBT VSCs are connected by a DC transmission line.

The four input control signals to the HVDC are M_r, PH_r, M_i, PH_i where M_r and M_i are the amplitude modulation ratio and PH_r and PH_i are phase angle of the control signals of each VSC respectively.

The AC side of each converter is connected to the line through a coupling transformer. The first VSC behaves as a rectifier. It regulates the DC link voltage and maintains the magnitude of the voltage at the connected terminal by two input control signals, Mr, PHr. The second VSC acts as a controlled voltage source, which controls power flow in HVDC feeder by controlling Mi, PHi.

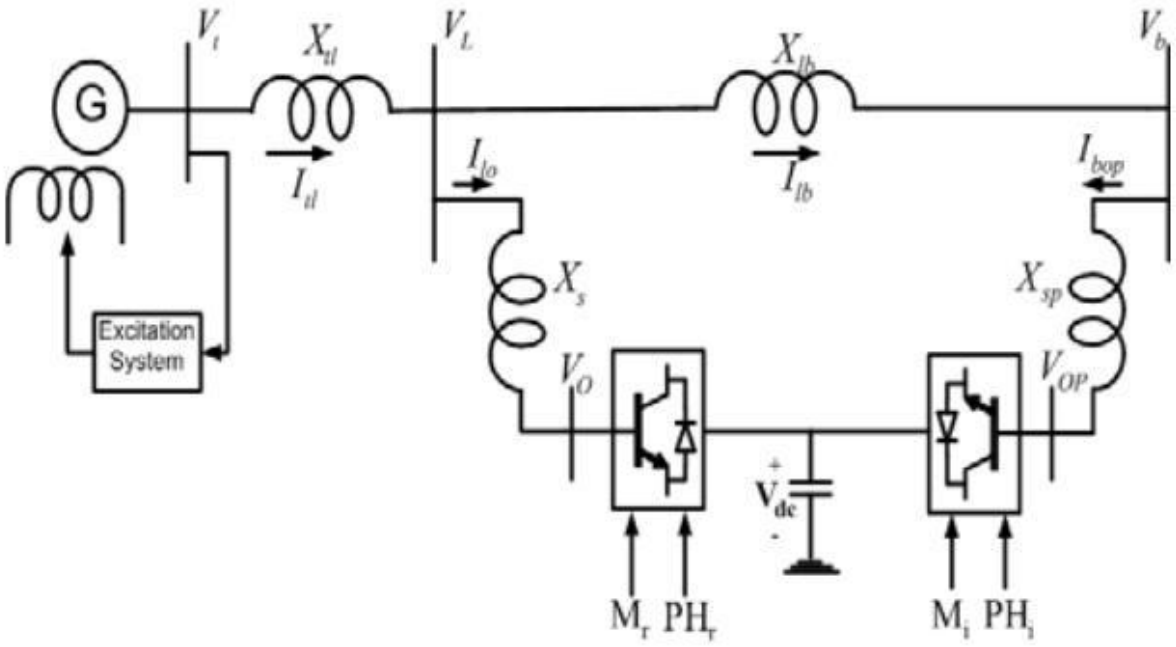

Figure 4.1: Configuration of the case study

4.3. Power system non linear model with HVDC

The dynamic model of the HVDC system is required in order to study the effect of the HVDC for enhancing the small signal stability of the power system. A non-linear dynamic model of the system is derived by disregarding the resistances of all the components of the system (generator, transformer, transmission lines, shunt and series converter transformers) and the transients of the transmission lines and transformers of the HVDC.

By applying Park's transformation and neglecting the resistance and transients of the coupling transformers, the HVDC can be modeled [6]:

$$\begin{bmatrix} V_{Ld} \\ V_{Lq} \end{bmatrix} = \begin{bmatrix} 0 & -X_s \\ X_s & 0 \end{bmatrix} \begin{bmatrix} I_{lod} \\ I_{loq} \end{bmatrix} + \begin{bmatrix} \frac{M_r V_{dc} \cos(PH_r)}{2} \\ \frac{M_r V_{dc} \sin(PH_r)}{2} \end{bmatrix}$$

$$\begin{bmatrix} V_{bd} \\ V_{bq} \end{bmatrix} = \begin{bmatrix} 0 & -X_{sp} \\ X_{sp} & 0 \end{bmatrix} \begin{bmatrix} I_{bopd} \\ I_{bopq} \end{bmatrix} + \begin{bmatrix} \frac{M_i V_{dc} \cos(PH_i)}{2} \\ \frac{M_i V_{dc} \sin(PH_i)}{2} \end{bmatrix}$$

$$C_{dc} \dot{V}_{dc} = [\frac{M_r}{2}(I_{lod} \cos(PH_r) + I_{loq} \sin(PH_r)) + \frac{M_i}{2}(I_{bopd} \cos(PH_i) + I_{bopq} \sin(PH_i))]$$

Where V_L, V_b, I_{lo}, I_{bo} are the middle bus voltage, infinite bus voltage, flowed current to rectifier and inverter respectively. C_{dc} and V_{dc} are the DC link capacitance and voltage, respectively.

The non-linear model of the SMIB system of Figure 5 is:

$$\dot{\delta} = \omega_b \omega$$

$$\dot{\omega} = \frac{\left(P_m - P_e - D\omega\right)}{M}$$

$$\dot{E}_q^{'} = \frac{(E_{fd} - (x_d - x_d^{'}) I_{td} - E_q^{'})}{T_{do}^{'}}$$

$$\dot{E}_{fd} = \frac{(K_A (V_{ref} - V_t) - E_{fd})}{T_A}$$

where $P_e = V_{td} I_{td} + V_{tq} I_{tq}$, $V_t = \sqrt{V_{td}^2 + V_{tq}^2}$, $V_{td} = x_q I_{tq}$,

$V_{tq} = E_q^{'} - x_d^{'} I_{td}$, $I_{td} = I_{lod} + I_{bd}$, $I_{tq} = I_{loq} + I_{bq}$

Pm and Pe are the input and output power, respectively; M and D the inertia constant and damping coefficient, respectively; ω_b the synchronous speed; δ and ω the rotor angle and speed, respectively; $E_q^{'}$, E_{fd} and V_t the generator internal, field and terminal voltages, respectively; T'_{d0} the open circuit field time constant; X_d, X'_d and X_q the d-axis, d-axis transient reactance, and q-axis reactance, respectively; K_A and T_A the exciter gain and time constant, respectively; V_{ref} the reference voltage.

Applying KCL and KVL, expressions for different currents and voltages of the system are determined:

$$\bar{V}_t = jX_{tl}\,\bar{I}_{tl} + \bar{V}_l$$

$$\bar{V}_t = jX_{tl}\,\bar{I}_{tl} + jX_{lb}\,\bar{I}_{lb} + \bar{V}_b$$

$$\bar{I}_{lb} = \bar{I}_{tl} - \frac{\bar{V}_t - jX_{tl}\,\bar{I}_{tl} - \bar{V}_o}{jX_s}$$

Using previous current and voltage expressions, the expression for armature current can be determined:

$$I_{tlq} = \frac{\frac{X_{lb}}{X_s}\frac{M_r}{2}V_{dc}\cos(PH_r) + V_b\sin(\delta)}{ZX_q + A}$$

$$I_{tld} = \frac{ZE_q^{'} - \frac{X_{lb}}{X_s}\frac{M_r}{2}V_{dc}\sin(PH_r)}{ZX_d^{'} + A} - \frac{V_b\cos(\delta)}{ZX_d^{'} + A}$$

Expression for inverter side current:

$$I_{bopd} = \frac{V_b\cos(\delta) - \frac{M_i}{2}V_{dc}\sin(PH_i)}{X_{sp}}$$

$$I_{bopq} = -\frac{V_b\sin(\delta) - \frac{M_i}{2}V_{dc}\cos(PH_i)}{X_{sp}}$$

4.4. Power system linearized model with HVDC

A linear dynamic model is obtained by linearising the non-linear model around an operating condition. However, the nonlinear dynamic model is linearized in order to select the most effective input control signals and design of phase compensator. The linearized model is given below :

$$\dot{\Delta\delta} = \omega_b \Delta\omega$$

$$\dot{\Delta\omega} = \frac{(\Delta P_m - \Delta P_e - D\Delta\omega)}{M}$$

$$\dot{\Delta E_q'} = \frac{(\Delta E_{fd} - (x_d - x_d')\Delta I_{td} - \Delta E_q')}{T_{do}'}$$

$$\dot{\Delta E}_{fd} = \frac{(-K_A \Delta V_t - \Delta E_{fd})}{T_A}$$

$$\dot{\Delta V}_{dc} = q_1 \Delta\delta + q_2 \Delta E_q' + q_3 \Delta V_{dc} + q_4 \Delta M_r + q_5 \Delta PH_r + q_6 \Delta M_i + q_7 \Delta PH_i$$

Where

$$\Delta V_t = K_5 \Delta\delta + K_6 \Delta E_q' + K_{Vdc} \Delta V_{dc} + K_{VM_r} \Delta M_r + K_{VPHr} \Delta PH_r$$

$$\Delta P_e = K_1 \Delta\delta + K_2 \Delta E_q' + K_{pdc} \Delta V_{dc} + K_{pMr} \Delta M_r + K_{pPHr} \Delta PH_r$$

$$\Delta E_q = K_3 \Delta E_q' + K_4 \Delta\delta + K_{qPHr} \Delta PH_r + K_{qMr} \Delta M_r + K_{qdc} \Delta V_{dc}$$

Where K_1-K_6, K_{pu}, K_{qu}, K_{vu}, K_q etc.are the linearization constants. The detailed expression for calculating these constants are represented in the Appendix.

4.5. Dynamic model in state-space form

The dynamic model of the system in state-space form is obtained from the transfer-function model as

$$\dot{\boldsymbol{X}} = \boldsymbol{AX} + \boldsymbol{Bu}$$

Where the state vector X, control vector U, A and B are :

$$\boldsymbol{X} = [\Delta\delta \quad \Delta\omega \quad \Delta E'_q \quad \Delta E_{fd} \quad \Delta V_{dc}]^T$$

$$U = [\Delta M_{\mathrm{r}}, \Delta \mathrm{PH}_{\mathrm{r}}, \Delta M_{\mathrm{i}}, \Delta \mathrm{PH}_{\mathrm{i}}]^T$$

$$A = \begin{bmatrix} 0 & \omega_b & 0 & 0 & 0 \\ -\frac{K_1}{M} & -\frac{D}{M} & -\frac{K_2}{M} & 0 & -\frac{K_{pdc}}{M} \\ -\frac{K_4}{T'_{do}} & 0 & -\frac{K_3}{T'_{do}} & \frac{1}{T'_{do}} & -\frac{K_{qdc}}{T'_{do}} \\ -\frac{K_A K_5}{T_A} & 0 & -\frac{K_A K_6}{T_A} & -\frac{1}{T_A} & -\frac{K_A K_{Vdc}}{T_A} \\ q_1 & 0 & q_2 & 0 & q_3 \end{bmatrix}$$

$$B = \begin{bmatrix} 0 & 0 & 0 & 0 \\ -\frac{K_{pMr}}{M} & -\frac{K_{pPHr}}{M} & 0 & 0 \\ -\frac{K_{qMr}}{T'_{do}} & -\frac{K_{qPHr}}{T'_{do}} & 0 & 0 \\ -\frac{K_A K_{VMr}}{T_A} & -\frac{K_A K_{VPHr}}{T_A} & 0 & 0 \\ q_4 & q_5 & q_6 & q_7 \end{bmatrix}.$$

The block diagram of the linearized dynamic model of the SMIB power system with HVDC is shown in Fig. 4.2.

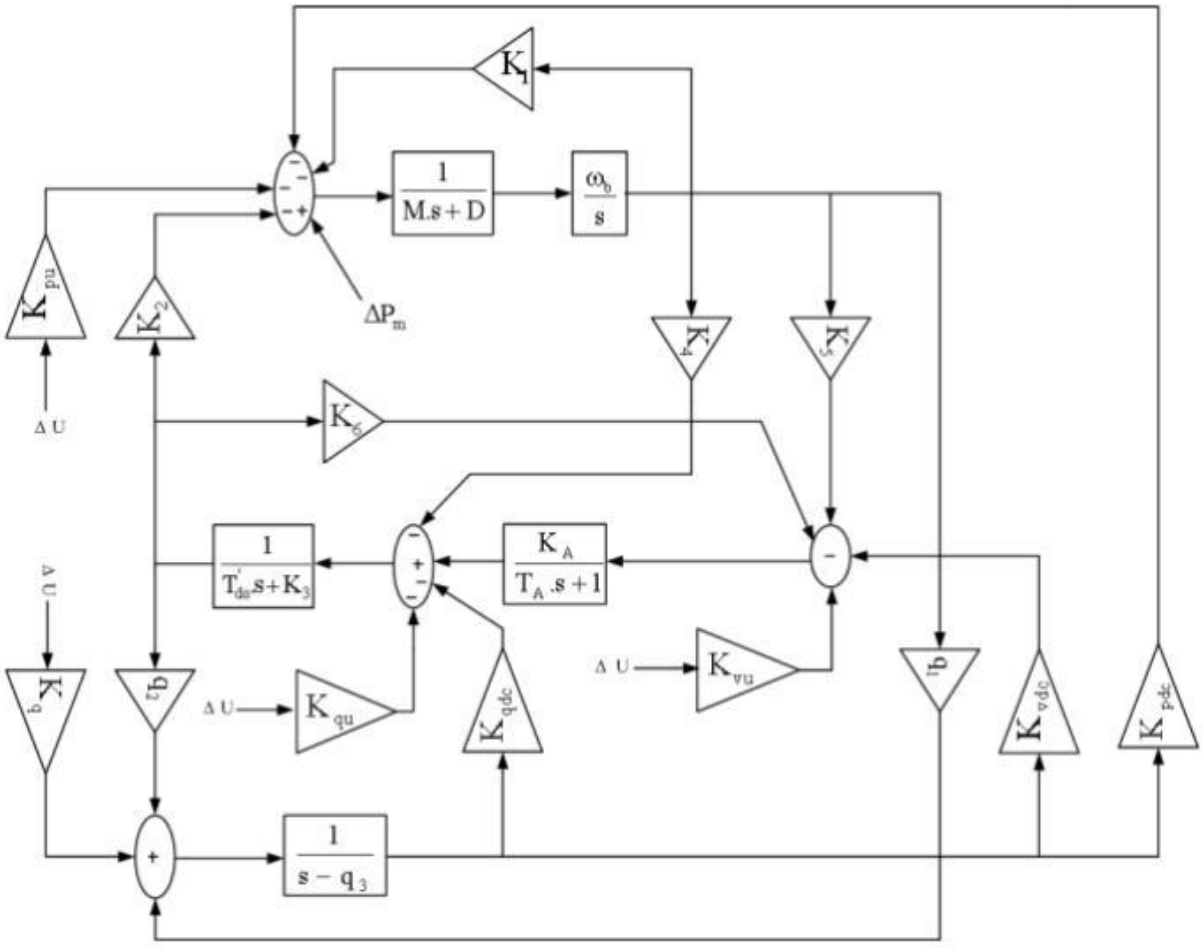

Figure 4.2: Phillips-Heffron model of power system installed with HVDC

In this figure $K_{pu}, K_{qu}, K_{vu}, K_q$ and ΔU are defined below:

$$K_{pu} = [K_{pMr}, K_{pPHr}, 0, 0]'$$

$$K_{qu} = [K_{qMr}, K_{qPHr}, 0, 0]'$$

$$K_{vu} = [K_{VMr}, K_{VPHr}, 0, 0]'$$

$$K_q = [q_4, q_5, q_6, q_7]'$$

$$\Delta U = [\Delta M_r, \Delta PH_r, \Delta M_i, \Delta PH_i]$$

4.6. Operating points calculation in steady condition

The initial d–q axes voltage and current components and torque angle are computed for the nominal operating condition ($\theta o = 15°$, $V_t = 1.0 \angle \theta o$, $V_b = 1.0 \angle 0$, $V_l = 1.0 \angle 0$, $P_t = 0.9$, $Q_t = 0.015$). These data are needed for computing the constants of the system model.

Step 1: First, we compute the parameters I_{tl} and E_{q0} using following two equations:

$$I_{tl}\angle\varphi_0 = \frac{P_t - jQ_t}{V_t^*}$$
$$E_{q0}\angle\delta_0 = V_t\angle\theta_0 + j\,X_q\,I_{tl}\angle\varphi_0$$

Step 2: By solving the four equations below we compute the parameters $V_{tq}, V_{td}, I_{tlq}, I_{tld}$ at the nominal operating condition. We obtained these equations from the phasor diagram of the system.

$$V_{tq} = |V_t|\cos(\delta_0 - \theta_0)$$
$$V_{td} = |V_t|\sin(\delta_0 - \theta_0)$$
$$I_{tlq} = |I_{tl}|\cos(\delta_0 - \varphi_0)$$
$$I_{tld} = |I_{tl}|\sin(\delta_0 - \varphi_0)$$

Step 3: Then we compute some other parameters using following equations:

$$P_{e0} = V_{td}\,I_{tld} + V_{tq}I_{tlq}$$

$$E_{fd0} = |E_q| + (X_d - X_q)\,I_{tld}$$

$$E'_{q0} = E_{fd0} - (X_d - X'_d)\,I_{tld}$$

Step 4: By applying KCL and KVL at different nodes of the system we obtained the following equations and using these equations we compute the rest of the voltage and current components.

$$V_l = V_t - j\,X_{tl}\,I_{tl}$$

$$I_{lb} = \frac{V_l - V_b}{j\,X_{lb}}$$

$$I_{lo} = I_{tl} - I_{lb}$$

$$V_0 = V_l - j\,X_s$$

Step 5: Using MATLAB ***fsolve*** function determine Mr and PHr fom the following two equations:

$$I_{tlq} = \frac{\frac{X_{lb}}{X_s}\frac{M_r}{2}V_{dc}\cos(PH_r) + V_b\sin(\delta)}{ZX_q + A}$$

$$I_{tld} = \frac{ZE_q^{'} - \frac{X_{lb}}{X_s}\frac{M_r}{2}V_{dc}\sin(PH_r)}{ZX_d^{'} + A} - \frac{V_b\cos(\delta)}{ZX_d^{'} + A}$$

Step 6: Assuming PHi=45°, determine the value of *Mi* from the following equation, *Mi* is selected such that dVdc is close to zero so that there exist no dynamics in the system initially. Iterative solution method is employed.

$$C_{dc}\dot{V}_{dc} = [\frac{M_r}{2}(I_{lod}\cos(PH_r) + I_{loq}\sin(PH_r)) + \frac{M_i}{2}(I_{bopd}\cos(PH_i) + I_{bopq}\sin(PH_i))]$$

4.7. MATLAB code for calculating initial condition, linearization constants and open loop eigenvalues:

```
clc;
clear all;
global xlb xs Vdc xq xdp Itlq Itld Eqp0 Vb0 xtl del0
phi=15*pi/180;
Vt=1.0*exp(j*phi);
Vt0=abs(Vt);
Vb0=1.0;
VL0=1.0;
Pt0=0.9;
Qt0=0.015;
Cdc=1;
td0=5.044;
w0=2*pi*60;

xsp=0.15;
xtl=0.15;
xlb=0.6;
xs=0.15;
xq=0.6;
xd=1.0;
xdp=0.3;
Itl=(Pt0-j*Qt0)/conj(Vt);
VL=Vt-j*xtl*Itl;
Ilb=(VL-Vb0)/(j*xlb);
Ilo=Itl-Ilb;
Vo=VL-j*xs;

Eq=Vt+j*xq*Itl;
del0=angle(Eq);
del_deg=angledim(del0,'radians','degrees');

ang_Itl=angle(Itl);
ang_Itl_deg=angledim(ang_Itl,'radians','degrees');

Vtq=Vt0*cos(del0-phi);
Vtd=Vt0*sin(del0-phi);

Itlq=abs(Itl)*cos(del0-ang_Itl);
Itld=abs(Itl)*sin(del0-ang_Itl);

Pe=Vtd*Itld+Vtq*Itlq;
Efd0=abs(Eq)+(xd-xq)*Itld;
Eqp0=Efd0-(xd-xdp)*Itld;

x0 = [1.0; 1.0];           % Make a starting guess at the solution
options=optimset('Display','iter');
[xy,fval] = fsolve(@myfun,x0,options) ; % Call solversd
Mr=xy(1);
PHr=xy(2);
PHi=45*pi/180;
```

```
ang_Ilo=angle(Ilo);
ang_Ilo_deg=angledim(ang_Ilo,'radians','degrees');

ang_Ilb=angle(Ilb);
ang_Ilb_deg=angledim(ang_Ilb,'radians','degrees');

Ilod=abs(Ilo)*sin(del0-ang_Ilo)
Iloq=abs(Ilo)*cos(del0-ang_Ilo)

Ilbd=abs(Ilb)*sin(del0-ang_Ilb)
Ilbq=abs(Ilb)*cos(del0-ang_Ilb)

dVdc=1;

for Mi=.01:.0001:1
   if dVdc >.001 || dVdc < 0

Ibopd=(Vb0*cos(del0)-(Mi/2)*Vdc*sin(PHi))/xsp;
Ibopq=-(Vb0*sin(del0)-(Mi/2)*Vdc*cos(PHi))/xsp;
dVdc=(((Mr/2)*Ilod*cos(PHr)+Iloq*sin(PHr))+((Mi/2)*Ibopd*cos(PHi)+Ibopq*sin(P
Hi)))/Cdc
Mi
   else
   end
end

Itd=Ilod+Ilbd;
Itq=Iloq+Ilbq;

Z=1+(xlb/xs);
A=xtl+xlb+(xtl*xlb/xs);

Ilod1=(Eqp0-xdp*Itd-(Mr/2)*Vdc*sin(PHr)-xtl*Itd)/xs;
Iloq1=((Mr/2)*Vdc*cos(PHr)-Itq*xtl-xq*Itq)/xs;

Mi=0.4886;
Pm=0.9;
w=1;
M=8;
Ka=120;
ta=0.015;
Vref=1;

B=A+Z*xq;
[A]=A+Z*xdp;
J=xd-xdp;
L=1/Vt0;
E=(xdp+xtl)/xs;
W=(xq+xtl)/xs;
G=sin(PHr)/xs;

cb=Eqp0+(xq-xdp);
c1=(Vb0*cos(del0)/B);
ca=(xq-xdp)*Itq;
```

```
c6=(Vb0*sin(del0)/[A]);
c5=Z/[A];
c4=xlb*Mr*cos(PHr)/(2*xs*B);
c9=(-(xlb/(2*xs))*Mr*sin(PHr))/[A];
c11=-E*c6;
c15=-W*c1;
c10=(1/xs)*(-(xdp+xtl)*c5+1);
c14=-(G*(Mr/2)+E*c9);
c17=-(W*c4-(Mr*cos(PHr))/(2*xs));

K1=cb*c1+ca*c6;
K2=Itq*(1+(xq-xdp)*c5);
K3=1+J*c5;
K4=J*c6;
K5=L*(Vtd*xq*c1-Vtq*xdp*c6);
K6=L*Vtq*(1-xdp*c5);
Kpdc=cb*c4+ca*c9;
Kqdc=J*c9;
Kvdc=L*(Vtd*xq*c4-Vtq*xdp*c9);

p11=Mr*cos(PHr)/(2*Cdc);
p13=Mr*sin(PHr)/(2*Cdc);
p15=Mi*cos(PHi)/(2*Cdc);
p17=Mi*sin(PHi)/(2*Cdc);
p1=-(Vb0*sin(del0)/xsp);
p5=-(Vb0*cos(del0)/xsp);
p3=-(Mi*sin(PHi))/(2*xsp);
p7=(Mi*cos(PHi))/(2*xsp);

q1=p11*c11+p13*c15+p15*p1+p17*p5;
q2=p11*c10;
q3=p11*c14+p13*c17+p15*p3+p17*p7;

F=[0 w0-1 0 0 0;(-K1/M) 0 (-K2/M) 0 (-Kpdc/M);(-K4/td0) 0 (-K3/(td0)) (1/td0)
(-Kqdc/td0);(-Ka*K5/ta) 0 (-Ka*K6/ta) (-1/ta) (-Ka*Kvdc/ta);q1 0 -q2 0 q3];

Q=eig(F)
```

subroutine function:

```
function f= myfun(xy)
global xlb xs Vdc xq xdp Itlq Itld Eqp0 Vb0 xtl del0
xlb=0.6;
xs=0.15;
Vdc=3;
xq=0.6;
xdp=0.3;
xtl=0.15;
Z=1+(xlb/xs);
A=xtl+xlb+(xtl*xlb/xs);
Mr=xy(1);
PHr=xy(2);
f(1)=(((xlb/xs)*(xy(1)/2)*Vdc*cos(xy(2))+Vb0*sin(del0))/(Z*xq+A))-Itlq;
f(2)=((-(xlb/xs)*(xy(1)/2)*Vdc*sin(xy(2))+Z*Eqp0)/(Z*xdp+A))-Itld-
(Vb0*cos(del0))/(Z*xdp+A);
f=f';
```

4.8. Simulation Result

Initial Condition

Table 4.1: List of operating points at steady condition

System parameter	Initial condition
$I_{tl}\angle\varphi_0$	0.8732 + 0.2184i
$E_{q0}\angle\delta_0$	0.8349 + 0.7827i
V_{tq}	0.8817
V_{td}	0.4719
I_{tlq}	0.7864
I_{tld}	0.4379
P_{e0}	0.9000
E_{fd0}	1.3196
E'_{q0}	1.0130
V_l	0.9987 + 0.1278i
I_{lb}	0.2131 + 0.0022i
I_{lo}	0.6602 + 0.2163i
V_0	0.9987 - 0.0222i
Mr	0.6877
PHr	0.8455
Mi	0.4886
Phi	0.7854

Open loop Eigenvalue analysis using system matrix [A] :

-54.3461
-12.7539
0.7459 + 3.5899i
0.7459 - 3.5899i
-1.5230

From the eigen values analysis it is very clear that the system is unstable without using power system stabilizer, since the real part of some eigen values are positive.

Chapter 5:
Damping Controller Design

5.1. HVDC based damping controller

The damping controller is designed to produce an electrical torque in phase with the speed deviation according to phase compensation method. The four control parameters of the HVDC (M_r, PH_r, M_i, PH_i) can be modulated in order to produce the damping torque.

In this paper all the four control signals are modulated in order to damping controller design. The speed deviation $\Delta\omega$ is considered as the input to the damping controller. The output of this controller is added to one of input control signals and the other signals have been considered zero, as a result the Phillips–Heffron model is single input and single output (SISO). However, an electrical torque in phase with the speed deviation is to be produced in order to improve damping of the system oscillations.

The structure of HVDC based damping controller is shown in Figure 5.1. This controller may be considered as a lead-lag compensator. It consists of gain, signal washout, and phase compensator blocks. The parameters of the damping controller are obtained using the phase compensation technique. The detailed step-by-step procedure for computing the parameters of the damping controllers using phase compensation technique is discussed in the next section.

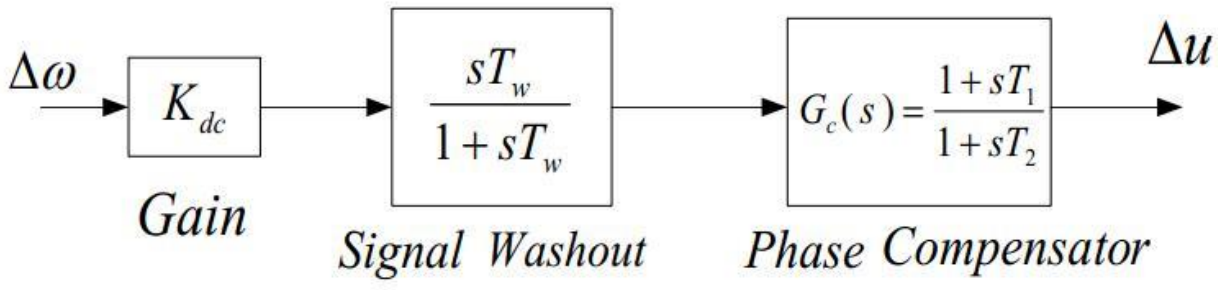

Figure 5.1: Structure of HVDC based damping controller

5.2. Controller design procedure

The detailed step-by-step procedure for computing the parameters of the damping controllers using phase compensation technique is discussed below [7].

Step 1: At first, the natural frequency of oscillations ω_n is calculated for the mechanical loop.

$$\omega_n = \sqrt{\frac{K_1 \omega_0}{M}}$$

where the amounts of ω_0 , K_1 *and* M has been presented in Appendix.

Step 2: Computation of $\angle GEPA$ at $s = j\omega_n$. Let it be γ.

Step 3: Design of phase lead-lag compensator G_c :

The phase lead-lag compensator G_c is designed to provide the required degree of phase compensation. For 100% phase compensation,

$$\angle G_C(j\omega_n) + \angle GEPA(j\omega_n) = 0$$

Assuming one lead-lag network, the transfer $T_1 = aT_2$ function of the phase compensator becomes,

$$G_C(s) = \frac{1 + saT_2}{1 + sT_2}$$

Since the phase angle compensated by the lead-lag network is equal to -γ , the parameters a *and* T_2 computed as,

$$a = \frac{1 + \sin(\gamma)}{1 - \sin(\gamma)}, \; T_2 = \frac{1}{\omega_n \sqrt{a}}$$

Step 4: The require gain setting Kdc for desired value of damping ratio ξ = 0.5 is obtained as,

$$K_{dc} = \frac{2\xi\omega_n M}{|G_C(s)||\gamma(s)|}$$

and $|G_C(s)|$ and $|\gamma(s)|$ are computed at $s = j\omega_n$.

The signal washout is the high pass filter that prevents steady changes in the speed from modifying the HVDC input parameter. The value of the washout time constant T_w should be high enough to allow signals associated with oscillations in rotor speed to pass unchanged. From the view point of the washout function, the value of T_w is not critical and may be in the range of 1s to 20s.

5.3. System dynamic model with controller

The dynamic model of the system with damping controller and different control input signals is represented below.

1. Dynamic model of the system with damping controller (control input Mr):

$$\begin{bmatrix} \Delta\dot{\delta} \\ \Delta\dot{\omega} \\ \Delta\dot{E}_q \\ \Delta\dot{E}_{fd} \\ \Delta\dot{V}_{dc} \\ \Delta\dot{Y}_1 \\ \Delta\dot{M}r \end{bmatrix} = \begin{bmatrix} 0 & \omega b & 0 & 0 & 0 & 0 & 0 \\ -K_1/M & -D/M & -K_2/M & 0 & -K_{pdc}/M & 0 & -K_{pmr}/M \\ -K_4/T_{do} & 0 & -K_3/T'_{do} & 1/T'_{do} & -K_{qdc}/Td & 0 & -K_{qmr}/T'_{do} \\ -K_AK_5/T_A & 0 & -K_AK_6/T_A & -1/T_A & -K_AK_{vdc}/T_A & 0 & -K_AK_{vmr}/T_A \\ q_1 & 0 & q_2 & 0 & q_3 & 0 & q_4 \\ -K_1K_{dc}/M & -DK_{dc}/M & -K_2K_{dc}/M & 0 & -K_{pdc}K_{dc}/M & -1/T_\omega & -K_{pmr}K_{dc}/M \\ -K_1K_{dc}T_1/MT_2 & -DK_{dc}T_1/MT_2 & -K_2K_{dc}T_1/MT_2 & 0 & -K_{pdc}K_{dc}T_1/MT_2 & (T_\omega - T_1)/T_\omega T_2 & -(M + K_{pmr}K_{dc}T_1)/MT_2 \end{bmatrix} \begin{bmatrix} \Delta\delta \\ \Delta\omega \\ \Delta E_q \\ \Delta E_{fd} \\ \Delta V_{dc} \\ \Delta Y_1 \\ \Delta Mr \end{bmatrix}$$

2. Dynamic model of the system with damping controller (control input PHr):

$$\begin{bmatrix} \Delta\dot{\delta} \\ \Delta\dot{\omega} \\ \Delta\dot{E}_q \\ \Delta\dot{E}_{fd} \\ \Delta\dot{V}_{dc} \\ \Delta\dot{Y}_1 \\ \Delta\dot{P}Hr \end{bmatrix} = \begin{bmatrix} 0 & \omega_b & 0 & 0 & 0 & 0 & 0 \\ -K_1/M & -D/M & -K_2/M & 0 & -K_{pdc}/M & 0 & -K_{p_{phr}}/M \\ -K_4/T'_{do} & 0 & -K_3/T'_{do} & 1/T'_{do} & -K_{qdc}/T'_{do} & 0 & -K_{q_{phr}}/T'_{do} \\ -K_AK_5/T_A & 0 & -K_AK_6/T_A & -1/T_A & -K_AK_{vdc}/T_A & 0 & -K_AK_{v_{phr}}/T_A \\ q_1 & 0 & q_A & 0 & q_3 & 0 & q_5 \\ -K_1K_{dc}/M & -DK_{dc}/M & -K_2K_{dc}/M & 0 & -K_{pdc}K_{dc}/M & -1/T_\omega & -K_{p_{Phr}}K_{dc}/M \\ -K_1K_{dc}T_1/MT_2 & -DK_{dc}T_1/MT_2 & -K_2K_{dc}T_1/MT_2 & 0 & -K_{pdc}K_{dc}T_1/MT_2 & (T_\omega - T_1)/T_\omega T_2 & -(M + K_{p_{Phr}}K_{dc}T_1)/MT_2 \end{bmatrix} \begin{bmatrix} \Delta\delta \\ \Delta\omega \\ \Delta E_q \\ \Delta E_{fd} \\ \Delta V_{dc} \\ \Delta Y_1 \\ \Delta PHr \end{bmatrix}$$

3. Dynamic model of the system with damping controller (control input Mi):

$$\begin{bmatrix} \Delta\dot{\delta} \\ \Delta\dot{\omega} \\ \Delta\dot{E}_q \\ \Delta\dot{E}_{fd} \\ \Delta\dot{V}_{dc} \\ \Delta\dot{Y}_1 \\ \Delta\dot{M}i \end{bmatrix} = \begin{bmatrix} 0 & \omega_b & 0 & 0 & 0 & 0 & 0 \\ -K_1/M & -D/M & -K_2/M & 0 & -K_{pdc}/M & 0 & 0 \\ -K_4/T'_{do} & 0 & -K_3/T'_{do} & 1/T'_{do} & -K_{qdc}/Td & 0 & 0 \\ -K_AK_5/T_A & 0 & -K_AK_6/T_A & -1/T_A & -K_AK_{vdc}/T_A & 0 & 0 \\ q_1 & 0 & q_2 & 0 & q_3 & 0 & q_6 \\ -K_1K_{dc}/M & -DK_{dc}/M & -K_2K_{dc}/M & 0 & -K_{pdc}K_{dc}/M & -1/T_\omega & 0 \\ -K_1K_{dc}T_1/MT_2 & -DK_{dc}T_1/MT_2 & -K_2K_{dc}T_1/MT_2 & 0 & -K_{pdc}K_{dc}T_1/MT_2 & (T_\omega - T_1)/T_\omega T_2 & -1/T_2 \end{bmatrix} \begin{bmatrix} \Delta\delta \\ \Delta\omega \\ \Delta E_q \\ \Delta E_{fd} \\ \Delta V_{dc} \\ \Delta Y_1 \\ \Delta Mi \end{bmatrix}$$

4. Dynamic model of the system with damping controller (control input PHi):

$$\begin{bmatrix} \Delta\dot{\delta} \\ \Delta\dot{\omega} \\ \Delta\dot{E}_q \\ \Delta\dot{E}_{fd} \\ \Delta\dot{V}_{dc} \\ \Delta\dot{Y}_1 \\ \Delta\dot{P}Hi \end{bmatrix} = \begin{bmatrix} 0 & \omega_b & 0 & 0 & 0 & 0 & 0 \\ -K_1/M & -D/M & -K_2/M & 0 & -K_{pdc}/M & 0 & 0 \\ -K_4/T'_{do} & 0 & -K_3/T'_{do} & 1/T'_{do} & -K_{qdc}/T_d & 0 & 0 \\ -K_AK_5/T_A & 0 & -K_AK_6/T_A & -1/T_A & -K_AKvdc/T_A & 0 & 0 \\ q_1 & 0 & q_2 & 0 & q_3 & 0 & q_7 \\ -K_1K_{dc}/M & -DK_{dc}/M & -K_2K_{dc}/M & 0 & -K_{pdc}K_{dc}/M & -1/T_\omega & 0 \\ -K_1K_{dc}T_1/MT_2 & -DK_{dc}T_1/MT_2 & -K_2K_{dc}T_1/MT_2 & 0 & -K_{pdc}K_{dc}T_1/MT_2 & (T_\omega - T_1)/T_\omega T_2 & -1/T_2 \end{bmatrix} \begin{bmatrix} \Delta\delta \\ \Delta\omega \\ \Delta E_q \\ \Delta E_{fd} \\ \Delta V_{dc} \\ \Delta Y_1 \\ \Delta PHi \end{bmatrix}$$

5.4. MATLAB code to assess system dynamic behavior with controller

```
clc;
clear all;
global xlb xs Vdc xq xdp Itlq Itld Eqp0 Vb0 xtl del0
phi=15*pi/180;
Vt=1.0*exp(j*phi);
Vt0=abs(Vt);
Vb0=1.0;
VL0=1.0;
Pt0=0.9;
Qt0=0.015;
Cdc=1;
td0=5.044;
w0=2*pi*60;

xsp=0.15;
xtl=0.15;
xlb=0.6;
xs=0.15;
xq=0.6;
xd=1.0;
xdp=0.3;
Itl=(Pt0-j*Qt0)/conj(Vt);
VL=Vt-j*xtl*Itl;
Ilb=(VL-Vb0)/(j*xlb);
Ilo=Itl-Ilb;
Vo=VL-j*xs;

Eq=Vt+j*xq*Itl;
del0=angle(Eq);
del_deg=angledim(del0,'radians','degrees');

ang_Itl=angle(Itl);
ang_Itl_deg=angledim(ang_Itl,'radians','degrees');

Vtq=Vt0*cos(del0-phi);
Vtd=Vt0*sin(del0-phi);

Itlq=abs(Itl)*cos(del0-ang_Itl);
Itld=abs(Itl)*sin(del0-ang_Itl);

Pe=Vtd*Itld+Vtq*Itlq;
Efd0=abs(Eq)+(xd-xq)*Itld;
Eqp0=Efd0-(xd-xdp)*Itld;

x0 = [1.0; 1.0];           % Make a starting guess at the solution
options=optimset('Display','iter');
[xy,fval] = fsolve(@myfun,x0,options) ; % Call solversd
Mr=xy(1);
PHr=xy(2);
PHi=45*pi/180;

ang_Ilo=angle(Ilo);
ang_Ilo_deg=angledim(ang_Ilo,'radians','degrees');
```

```
ang_Ilb=angle(Ilb);
ang_Ilb_deg=angledim(ang_Ilb,'radians','degrees');

Ilod=abs(Ilo)*sin(del0-ang_Ilo);
Iloq=abs(Ilo)*cos(del0-ang_Ilo);

Ilbd=abs(Ilb)*sin(del0-ang_Ilb);
Ilbq=abs(Ilb)*cos(del0-ang_Ilb);

dVdc=1;

for Mi=.01:.0001:1
   if dVdc >.001 || dVdc < 0

Ibopd=(Vb0*cos(del0)-(Mi/2)*Vdc*sin(PHi))/xsp;
Ibopq=-(Vb0*sin(del0)-(Mi/2)*Vdc*cos(PHi))/xsp;
dVdc=(((Mr/2)*Ilod*cos(PHr)+Iloq*sin(PHr))+((Mi/2)*Ibopd*cos(PHi)+Ibopq*sin(P
Hi)))/Cdc;
Mi;
   else
   end
end

Itd=Ilod+Ilbd;
Itq=Iloq+Ilbq;

Z=1+(xlb/xs);
A=xtl+xlb+(xtl*xlb/xs);

Ilod1=(Eqp0-xdp*Itd-(Mr/2)*Vdc*sin(PHr)-xtl*Itd)/xs;
Iloq1=((Mr/2)*Vdc*cos(PHr)-Itq*xtl-xq*Itq)/xs;

Mi=0.4886;
Pm=0.9;
w=1;
M=8;
Ka=120;
ta=0.015;
Vref=1;

B=A+Z*xq;
[A]=A+Z*xdp;
J=xd-xdp;
L=1/Vt0;
E=(xdp+xtl)/xs;
W=(xq+xtl)/xs;
G=sin(PHr)/xs;
tw=10;

T1=0.45;
T2=0.45;
Kdc=-38;
```

```
deldelta(1)=0;
delw(1)=0;
delEqp(1)=0;
delEfd(1)=0;
delVdc(1)=0;
delMr(1)=0;
delPhr(1)=0;
delPhi(1)=0;
delMi(1)=0;
dely1(1)=0;

cb=Eqp0+(xq-xdp);
c1=(Vb0*cos(del0)/B);
ca=(xq-xdp)*Itq;
c6=(Vb0*sin(del0)/[A]);
c5=Z/[A];
c4=xlb*Mr*cos(PHr)/(2*xs*B);
c9=(-(xlb/(2*xs))*Mr*sin(PHr))/[A];
c11=-E*c6;
c15=-W*c1;
c10=(1/xs)*(-(xdp+xtl)*c5+1);
c14=-(G*(Mr/2)+E*c9);
c17=-(W*c4-(Mr*cos(PHr))/(2*xs));
c3=xlb*Vdc*cos(PHr)/(2*xs*B);
c8=-xlb*Vdc*sin(PHr)/(2*xs*[A]);
c13=-(E*c8+G*Vdc/2);
c18=-(W*c3-(Vdc*cos(PHr)/(2*xs)));
c2=-(xlb*Mr*Vdc*sin(PHr)/(2*xs*B));
c7=1/[A]*(-xlb*Mr*Vdc*cos(PHr)/(2*xs));
c12=-(E*c7+Mr*Vdc*cos(PHr)/(2*xs));
c16=-(W*c2+Mr*Vdc*sin(PHr)/(2*xs));

K1=cb*c1+ca*c6;
K2=Itq*(1+(xq-xdp)*c5);
K3=1+J*c5;
K4=J*c6;
K5=L*(Vtd*xq*c1-Vtq*xdp*c6);
K6=L*Vtq*(1-xdp*c5);
Kpdc=cb*c4+ca*c9;
Kqdc=J*c9;
Kvdc=L*(Vtd*xq*c4-Vtq*xdp*c9);
Kpmr=cb*c3+c8*ca;
Kqmr=J*c8;
Kvmr=L*(Vtd*xq*c3-Vtq*xdp*c8);
KpPhr=cb*c2+ca*c7;
KqPhr=J*c7;
KvPhr=L*(Vtd*xq*c2-Vtq*xdp*c7);

p11=Mr*cos(PHr)/(2*Cdc);
p13=Mr*sin(PHr)/(2*Cdc);
p15=Mi*cos(PHi)/(2*Cdc);
p17=Mi*sin(PHi)/(2*Cdc);
p1=-(Vb0*sin(del0)/xsp);
p5=-(Vb0*cos(del0)/xsp);
p3=-(Mi*sin(PHi))/(2*xsp);
p7=(Mi*cos(PHi))/(2*xsp);
```

```
p9=(Ilod*cos(PHr)+Iloq*sin(PHr))/(2*Cdc);
p12=-(Mr*sin(PHr)*Ilod/(2*Cdc));
p14=(Mr*cos(PHr)*Iloq/(2*Cdc));
p124=p12+p14;
p10=(Ibopd*cos(PHi)+Ibopq*sin(PHi))/(2*Cdc);
p4=-Vdc*sin(PHi)/(2*xs);
p8=Vdc*cos(PHi)/(2*xsp);
p2=-Mi*Vdc*cos(PHi)/(2*xsp);
p6=-Mi*Vdc*sin(PHi)/(2*xsp);
p18=Mi*cos(PHi)*Ibopq/(2*Cdc);
p16=-Mi*sin(PHi)*Ibopq/(2*Cdc);
p186=p18+p16;

q1=p11*c11+p13*c15+p15*p1+p17*p5;
q2=p11*c10;
q3=p11*c14+p13*c17+p15*p3+p17*p7;
q4=p9+p11*c13+p13*c18;
q5=p11*c12+p13*c16+p124;
q6=p10+p15*p4+p17*p8;
q7=p15*p2+p17*p6+p186;

Ts=.001;
tsim=15;
t=zeros(1,tsim/Ts);
flt_strt=1.0;
flt_end=1.1;
 for i=1:length(t)

 t(i+1)=t(i)+Ts;

if i>flt_strt/Ts &&  i<flt_end/Ts
       dis=0.1;
    else
        dis=0;
 end

deldelta(i+1)= deldelta(i)+ Ts*(w0*delw(i));
delw(i+1)=delw(i)+Ts*(-(K1/M)*deldelta(i)-(K2/M)*delEqp(i)-
(Kpdc/M)*delVdc(i)-(Kpmr/M)*delMr(1)-(KpPhr/M)*delPhr(i)+dis);
delEqp(i+1)=delEqp(i)+Ts*(-(K4/td0)*deldelta(i)-
(K3/td0)*delEqp(i)+(1/td0)*delEfd(i)-(Kqdc/td0)*delVdc(i)-
(Kqmr/td0)*delMr(1)-(KqPhr/td0)*delPhr(i));
delEfd(i+1)=delEfd(i)+Ts*(-(Ka*K5/ta)*deldelta(i)-(Ka*K6/ta)*delEqp(i)-
(1/ta)*delEfd(i)-(Ka*Kvdc/ta)*delVdc(i)-(Ka*Kvmr/ta)*delMr(1)-
(Ka*KvPhr/ta)*delPhr(i));
delVdc(i+1)=delVdc(i)+Ts*(q1*deldelta(i)-
q2*delEqp(i)+q3*delVdc(i)+q4*delMr(1)+q5*delPhr(i)+q6*delMi(1)+q7*delPhi(1));

dely1(i+1)=dely1(i)+Ts*(-(K1*Kdc/M)*deldelta(i)-(K2*Kdc/M)*delEqp(i)-
(Kpdc*Kdc/M)*delVdc(i)-(1/tw)*dely1(i)-(KpPhr*Kdc/M)*delPhr(i));
delPhr(i+1)=delPhr(i)+Ts*(-(K1*Kdc*T1/(M*T2))*deldelta(i)-
(K2*Kdc*T1/(M*T2))*delEqp(i)-(Kpdc*Kdc*T1/(M*T2))*delVdc(i)+((tw-
T1)/(T2*tw))*dely1(i)-((KpPhr*Kdc*T1/(M*T2))+(1/T2))*delPhr(i));
 end
```

5.5. Simulation result

Eigenvalue Analysis

The system eigenvalues with the proposed controllers are given in Table 5.1. It is clear that the open loop system is unstable but the proposed controllers stabilize the system. Obviously the electromechanical–mode eigenvalues have been shifted to the left in s-plane and the system damping with the proposed method greatly improved and enhanced.

Table 5.1: system eigenvalues with damping controller

	Control input signal		
	PHr	*Mr*	*PHi*
Closed loop Eigenvalue	-54.5832 -10.5419 -6.4414 -0.5345 + 1.8950i -0.5345 - 1.8950i -0.0990 -2.2222	-56.1561 -2.0702 + 5.3291i -2.0702 - 5.3291i -1.9136 + 2.0234i -1.9136 - 2.0234i -0.1000 -2.0000	1.0e+002 * -1.0190 -0.5816 -0.0174 + 0.0564i -0.0174 - 0.0564i -0.0180 + 0.0191i -0.0180 - 0.0191i -0.0010

Non linear time domain simulation

The efficiency of the proposed control system was evaluated for small-signal disturbance at t=1s by applying imbalance of 0.1 pu between generation and consumption power at nominal load and the results are compared for different control inputs of the damping controller.

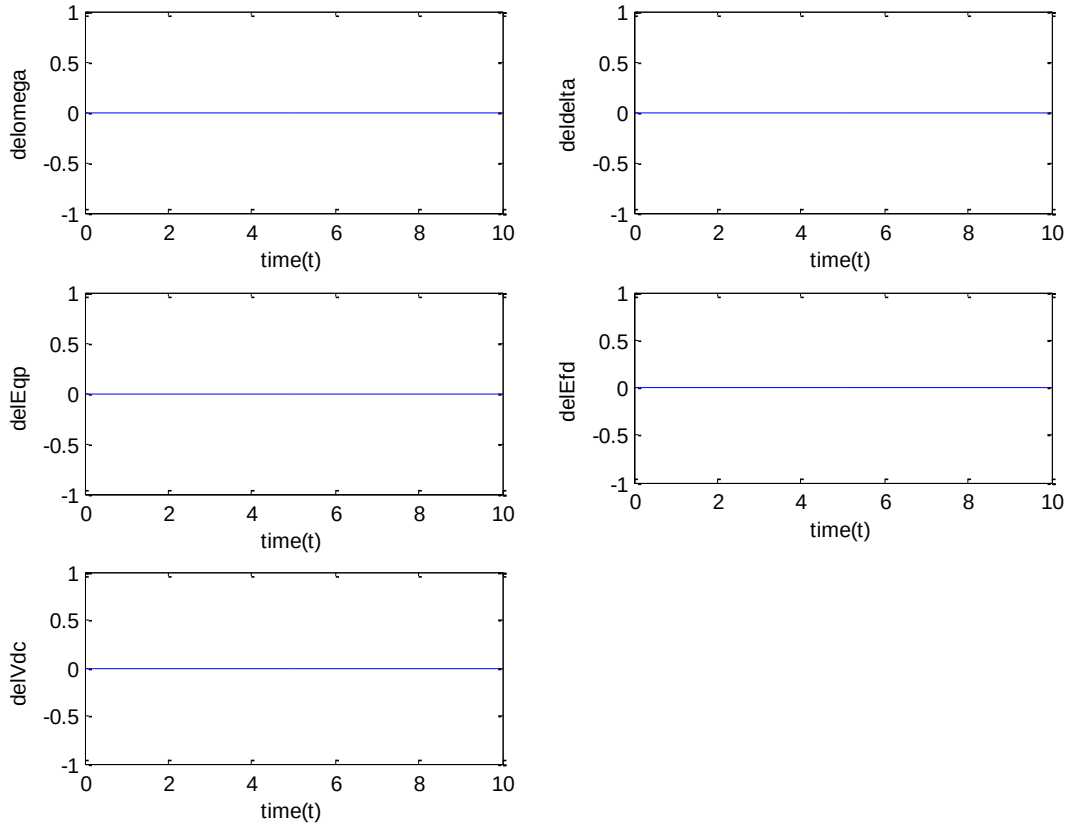

Figure 5.2: Dynamic response of the system with controller (no disturbance applied)

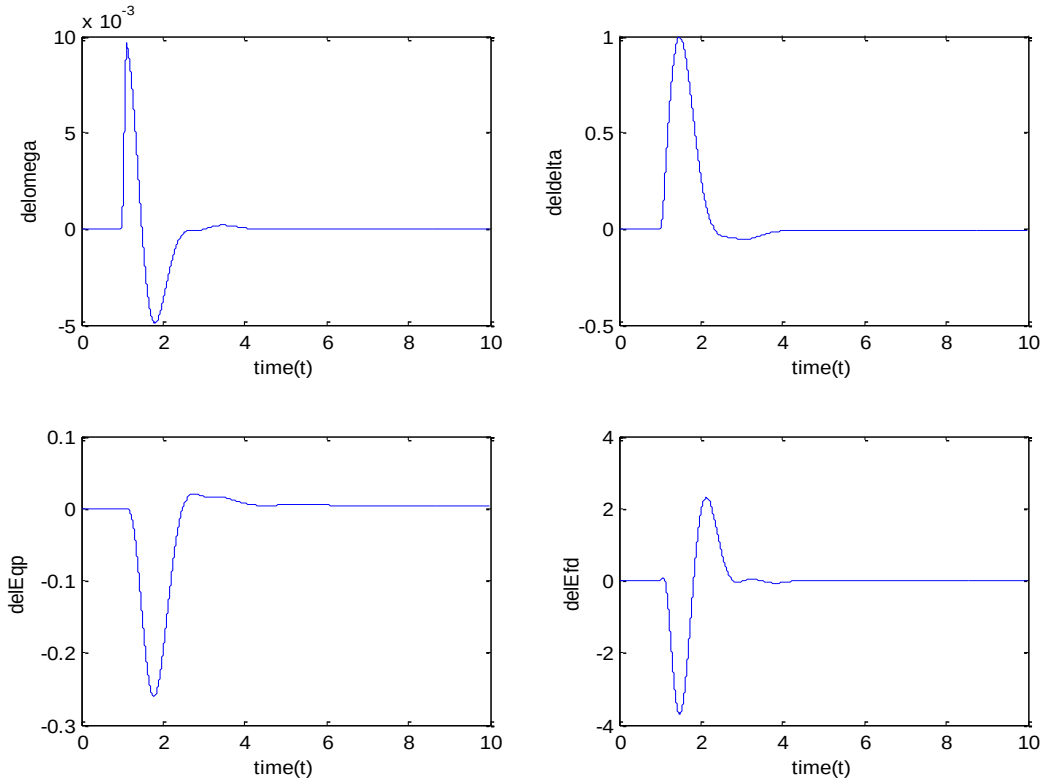

Figure 5.3: Dynamic response of the system with controller; control input signal Mr (disturbance applied at 1s)

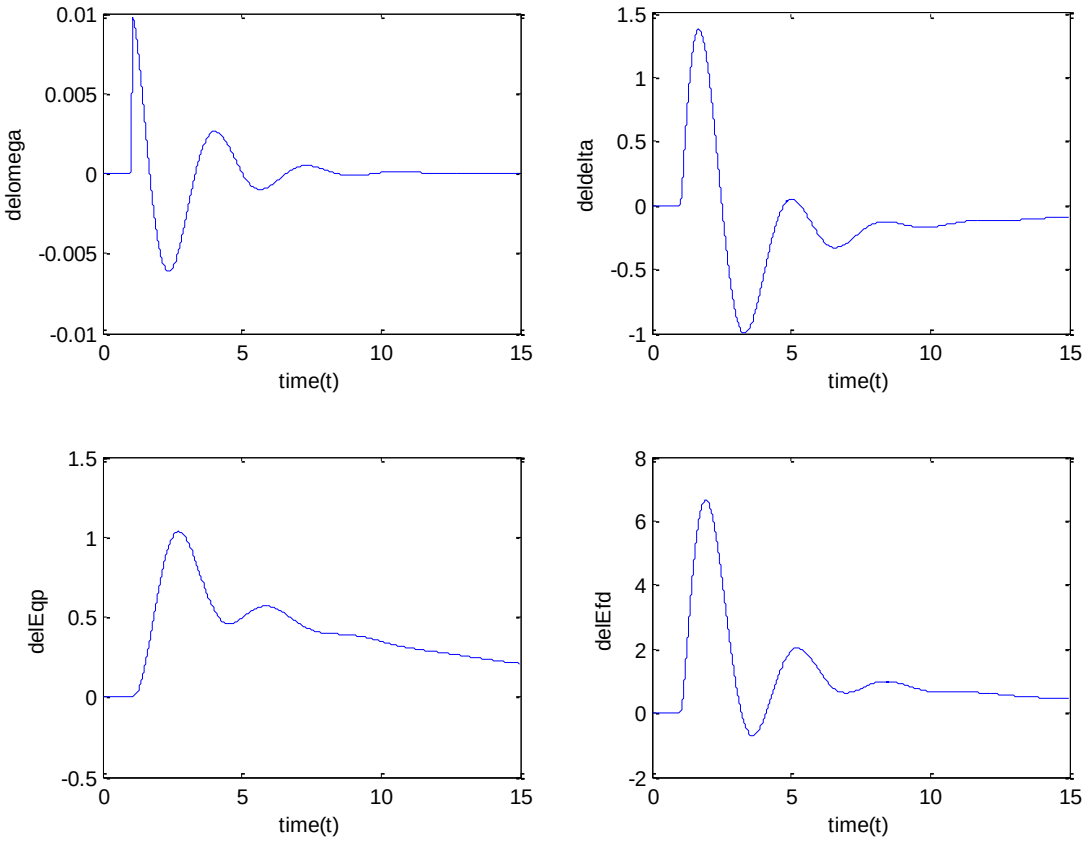

Figure 5.4: Dynamic response of the system with controller; control input signal PHr (disturbance applied at 1s)

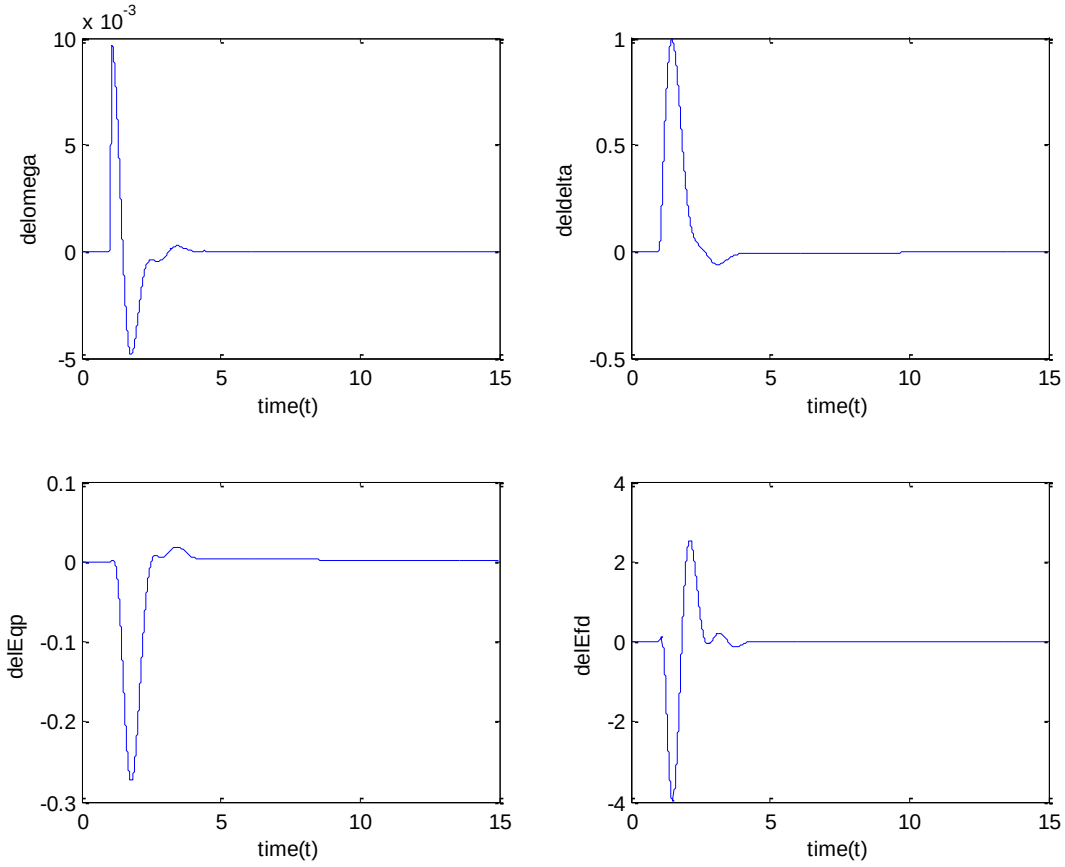

Figure 5.5: Dynamic response of the system with controller; control input signal PHi (disturbance applied at 1s)

5.6. Conclusion

- In this paper, a dynamic model for an AC-DC power system is considered and damping controller is designed to improve power system stability and oscillation damping.
- A comprehensive approach to designing damping controller has been presented.
- The relative effectiveness of HVDC control signals in damping low-frequency oscillations has been examined. Investigations have revealed that HVDC control signal Mi is ineffective in damping oscillations.
- Simulations and experiment results indicate that the proposed controller can effectively enhance the dynamic performance of the power system.

Appendix

Appendix 1

The test system parameters are:

Machine and exciter: $X_d = 1, X_q = 0.6, X'_d = 0.3, D = 0, M = 8,$ $T'_{do} = 5.044, freq = 60, v_{ref} = 1, K_A = 120,$ $T_A = 0.015$

Transmission line and transformer reactance: $X_{tl} = 0.15, X_{lb} = 0.6,$ $X_{sp} = X_s = 0.15$

BtB VSC HVDC: $V_{dc} = 3, C_{dc} = 1$

Appendix 2

Coefficients are:

$$Z = 1 + \frac{X_{lb}}{X_s},\ A = X_{tl} + X_{lb} + \frac{X_{tl} X_{lb}}{X_s}$$

$$[A] = A + ZX'_d,\ [B] = A + ZX_q$$

$$C_1 = \frac{V_b \cos(\delta)}{[B]},\ C_2 = -\frac{X_{lb} M_r V_{dc} \sin(PHr)}{2X_s[B]}$$

$$C_3 = \frac{X_{lb} V_{dc} \cos(PHr)}{2X_s[B]},\ C_4 = \frac{X_{lb} M_r \cos(PHr)}{2X_s[B]}$$

$$C_5 = \frac{Z}{[A]},\ C_6 = \frac{V_b \sin(\delta)}{[A]}$$

$$C_7 = -\frac{X_{lb} M_r V_{dc} \cos(PHr)}{2X_s[A]},\ C_8 = -\frac{X_{lb} V_{dc} \sin(PHr)}{2X_s[A]}$$

$$C_9 = -\frac{X_{lb} M_r \sin(PHr)}{2X_s[A]},\ C_b = E'_q + (X_q - X'_d)$$

$$C_a = (X_q - X'_d) I_{tlq},\ K_1 = C_b C_1 + C_a C_6$$

$$K_2 = I_{tlq}(1 + (X_q - X'_d) C_5),\ K_{pdc} = C_b C_4 + C_a C_9$$

$$K_{pMr} = C_b C_3 + C_a C_8,\ K_{pPHr} = C_b C_2 + C_a C_7$$

$$X_d - X'_d = J,\ K_3 = 1 + JC_5,\ K_4 = JC_6,\ K_{qPHr} = JC_7$$

$$K_{qMr} = JC_8,\ K_{qdc} = JC_9,\ L = \frac{1}{V_t}$$

$$K_5 = L(V_{td} X_q C_1 - V_{tq} X'_d C_6)$$

$$P_7 = \frac{M_i \cos(PHi)}{2X_{sp}},\ P8 = \frac{V_{dc} \cos(PHi)}{2X_{sp}}$$

$$P_9 = \frac{I_{lod} \cos(PHr) + I_{loq} \sin(PHr)}{2C_{dc}}$$

$$P10 = \frac{I_{bopd} \cos(PHi) + I_{bopq} \sin(PHi)}{2C_{dc}}$$

$$P_{11} = \frac{M_r \cos(PHr)}{2C_{dc}},\ P_{12} = -\frac{M_r \sin(PHr) I_{lod}}{2C_{dc}}$$

$$P_{13} = \frac{M_r \sin(PHr)}{2C_{dc}},\ P_{14} = \frac{M_r \cos(PHr) I_{loq}}{2C_{dc}}$$

$$P_{15} = \frac{M_i \cos(PHi)}{2C_{dc}},\ P_{16} = -\frac{M_i \sin(PHi) I_{bopd}}{2C_{dc}}$$

$$P_{17} = \frac{M_i \sin(PHi)}{2C_{dc}},\ P_{18} = \frac{M_i \cos(PHi) I_{bopq}}{2C_{dc}}$$

$$P_{124} = P_{12} + P_{14},\ P_{186} = P_{18} + P_{16}$$

$$q_1 = P_{11}C_{11} + P_{13}C_{15} + P_{15}P_1 + P_{17}P_5$$

$$q_2 = P_{11}C_{10},\ q_3 = P_{11}C_{14} + P_{13}C_{17} + P_{15}P_3 + P_{17}P_7$$

$$q_4 = P_9 + P_{11}C_{13} + P_{13}C_{18},\ q_5 = P_{11}C_{12} + P_{13}C_{16} + P_{124}$$

$$q_6 = P_{10} + P_{15}P_4 + P_{17}P_8$$

$$q_7 = P_{15}P_2 + P_{17}P_6 + P_{186}$$

$$K_6 = LVtq(1 - X'_d C_5),\ K_{Vdc} = L(V_{td} X_q C_4 - V_{tq} X'_d C_9)$$

$$K_{VMr} = L(V_{td} X_q C_3 - V_{tq} X'_d C_8)$$

$$K_{VPHr} = L(V_{td} X_q C_2 - V_{tq} X'_d C_7),\ E = \frac{X'_d + X_{tl}}{X_s}$$

$$G = \frac{\sin(PHr)}{X_s},\ C_{10} = \frac{1}{X_s}(-(X'_d + X_{tl})C_5 + 1)$$

$$C_{11} = -EC_6,\ C_{12} = -(EC_7 + \frac{M_r V_{dc} \cos(PHr)}{2X_s})$$

$$C_{13} = -(EC_8 + \frac{GV_{dc}}{2}),\ C_{14} = -(G\frac{M_r}{2} + EC_9)$$

$$W = \frac{X_q + X_{tl}}{X_s},\ C_{15} = -WC_1$$

$$C_{16} = -(WC_2 + \frac{M_r V_{dc} \sin(PHr)}{2X_s}),$$

$$C_{17} = -(WC_4 - \frac{M_r \cos(PHr)}{2X_s}),\ P_1 = -\frac{V_b \sin(\delta)}{X_{sp}}$$

$$C_{18} = -(WC_3 - \frac{V_{dc} \cos(PHr)}{2X_s}),\ P_2 = -\frac{M_i V_{dc} \cos(PHi)}{2X_{sp}}$$

$$P_3 = -\frac{M_i \sin(PHi)}{2X_{sp}},\ P_4 = -\frac{V_{dc} \sin(PHi)}{2X_{sp}}$$

$$P_5 = -\frac{V_b \cos(\delta)}{X_{sp}},\ P_6 = -\frac{M_i V_{dc} \sin(PHi)}{2X_{sp}}$$

REFERENCES

[1] Kundur, Prabha, et al. "Definition and classification of power system stability IEEE/CIGRE joint task force on stability terms and definitions." *Power Systems, IEEE Transactions on* 19.3 (2004): 1387-1401.

[2] HILAWIE, AHADU. *INVESTIGATION OF VSC-HVDC SYSTEM FOR DYNAMIC PERFORMANCE IMPROVEMENT OF EEPCO HIGH VOLTAGE GRID*. Diss. Institute of Technology, School of Graduate Studies, Addis Ababa University, 2011.

[3] Ramadan, Haitham Saad Mohamed. "Non-linear control and stabilization of VSC-HVDC transmission systems." (2012).

[4] Okba, M.H.; Saied, M.H.; Mostafa, M. Z.; Abdel- Moneim, T. M., "High voltage direct current transmission - A review, part I," *Energytech, 2012 IEEE*, vol., no., pp.1,7, 29-31 May 2012

[5] Banaei, M. R., and N. Taheri. "An adaptive neural damping controller for HVDC transmission systems." *European Transactions on Electrical Power* 21.1 (2011): 910-923

[6] Tabatabaei, N. M., N. Taheri, and N. S. Boushehri. "Damping Function of Back to Back HVDC Based Voltage Source Converter." *International Journal on Technical and Physical Problems of Engineering (IJTPE)* 4 (2010): 82-87.

[7] Tabatabaei, N. M., et al. "SVD-UPFC Based Designation of Versatile Controllers to Damp Low Frequency Oscillations." *International Journal on Technical and Physical Problems of Engineering (IJTPE)* 9: 59-67.

[8] Padiyar, K. R. *Power system dynamics*. BS publications, 2008.

[9] Kundur, Prabha. *Power system stability and control*. Tata McGraw-Hill Education, 1994.

[10] Nise, Norman S. *Control systems engineering*. Vol.5. Hoboken, NJ: Wiley, 2008.

[11] Latorre, Hector. *Modeling and Control of VSC-HVDC Transmissions*. Diss. KTH, 2011.